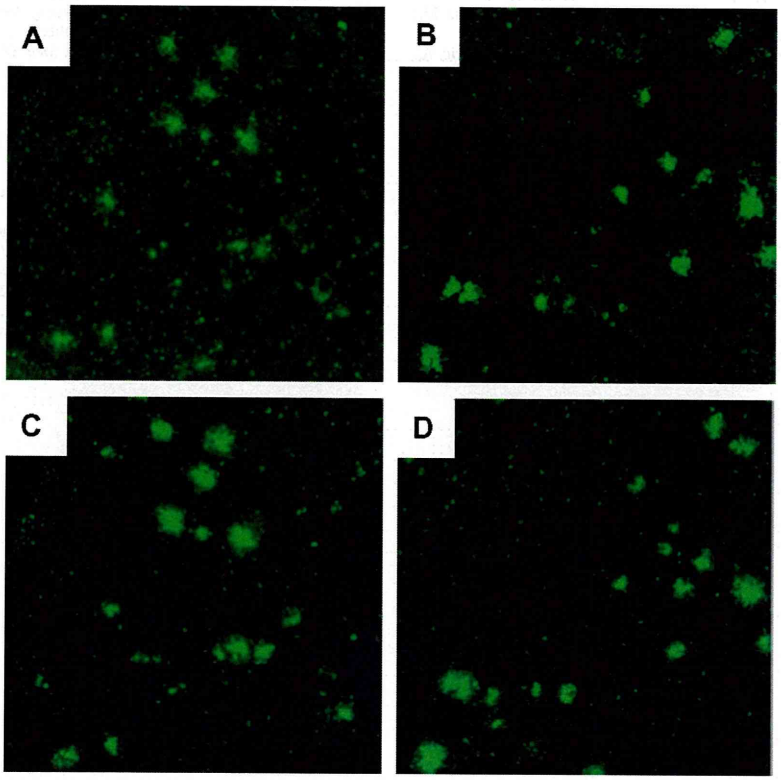

Figure 3. Fluorescent staining of the flavone derivative **9** (A), and aurone derivative **19** (B) in Tg2576 mouse brain. Labeled plaques were confirmed by staining the adjacent sections with thioflavin S (C and D).

Table 2
Biodistribution of radioactivity after injection of [^{99m}Tc]BAT-FL and [^{99m}Tc]BAT-AR in normal mice[a]

Organ	Time after injection (min)			
	2	10	30	60
[^{99m}Tc]BAT-FL (**10**)				
Blood	1.90 (0.08)	0.80 (0.16)	0.41 (0.06)	0.28 (0.06)
Liver	19.35 (1.30)	24.75 (3.45)	27.73 (3.30)	24.12 (3.08)
Kidney	9.70 (0.83)	5.56 (0.84)	2.38 (0.30)	1.40 (0.20)
Intestine[b]	4.54 (0.42)	11.36 (1.88)	26.61 (3.93)	42.67 (2.98)
Spleen	3.24 (0.61)	2.21 (0.31)	1.04 (0.42)	0.45 (0.07)
Lung	11.42 (2.10)	3.84 (0.57)	1.70 (0.24)	1.07 (0.16)
Stomach[b]	0.90 (0.15)	1.36 (0.55)	1.52 (0.67)	2.45 (1.04)
Pancreas	4.41 (0.29)	4.31 (0.35)	1.89 (0.15)	0.84 (0.17)
Heart	12.00 (1.16)	3.12 (0.51)	0.99 (0.18)	0.44 (0.09)
Brain	0.64 (0.07)	0.57 (0.14)	0.36 (0.01)	0.23 (0.04)
[^{99m}Tc]BAT-AR (**20**)				
Blood	1.56 (0.16)	0.71 (0.07)	0.35 (0.04)	0.21 (0.04)
Liver	17.76 (1.51)	17.77 (1.70)	15.17 (0.95)	12.96 (1.48)
Kidney	11.50 (0.73)	8.77 (1.15)	4.83 (0.77)	3.28 (1.52)
Intestine[b]	6.78 (0.78)	26.20 (2.45)	46.06 (3.17)	55.33 (7.42)
Spleen	2.87 (0.30)	1.92 (0.47)	0.70 (0.07)	0.35 (0.15)
Lung	6.10 (1.15)	3.25 (0.78)	1.63 (0.42)	0.85 (0.18)
Stomach[b]	1.03 (0.13)	1.63 (0.25)	1.88 (0.11)	1.69 (0.49)
Pancreas	5.85 (1.09)	4.20 (0.68)	1.53 (0.54)	0.60 (0.30)
Heart	12.30 (1.21)	3.26 (0.43)	1.15 (0.30)	0.40 (0.09)
Brain	0.79 (0.12)	0.70 (0.05)	0.27 (0.06)	0.11 (0.04)

[a] Each value represents the mean (SD) for 3–6 mice at each interval. Expressed as % injected dose per gram.
[b] Expressed as % injected dose per organ.

Acknowledgments

This study was supported by the Program for Promotion of Fundamental Studies in Health Sciences of the National Institute of Biomedical Innovation (NIBIO), a Health Labour Sciences Research Grant, and a Grant-in-aid for Young Scientists (A) and Exploratory Research from the Ministry of Education, Culture, Sports, Science and Technology, Japan.

Supplementary data

Supplementary data (procedure for the preparation of ^{99m}Tc/Re complexes, in vitro binding assay, in vitro fluorescent staining using Tg2576 mouse brain sections, and biodistribution experiments) associated with this article can be found, in the online version, at doi:10.1016/j.bmcl.2010.08.004.

References and notes

1. Selkoe, D. J. *Physiol. Rev.* **2001**, *81*, 741.
2. Selkoe, D. J. *Nat. Biotechnol.* **2000**, *18*, 823.
3. Mathis, C. A.; Wang, Y.; Klunk, W. E. *Curr. Pharm. Des.* **2004**, *10*, 1469.
4. Nordberg, A. *Lancet Neurol.* **2004**, *3*, 519.
5. Mathis, C. A.; Wang, Y.; Holt, D. P.; Huang, G. F.; Debnath, M. L.; Klunk, W. E. *J. Med. Chem.* **2003**, *46*, 2740.
6. Klunk, W. E.; Engler, H.; Nordberg, A.; Wang, Y.; Blomqvist, G.; Holt, D. P.; Bergstrom, M.; Savitcheva, I.; Huang, G. F.; Estrada, S.; Ausen, B.; Debnath, M. L.; Barletta, J.; Price, J. C.; Sandell, J.; Lopresti, B. J.; Wall, A.; Koivisto, P.; Antoni, G.; Mathis, C. A.; Langstrom, B. *Ann. Neurol.* **2004**, *55*, 306.
7. Ono, M.; Wilson, A.; Nobrega, J.; Westaway, D.; Verhoeff, P.; Zhuang, Z. P.; Kung, M. P.; Kung, H. F. *Nucl. Med. Biol.* **2003**, *30*, 565.
8. Verhoeff, N. P.; Wilson, A. A.; Takeshita, S.; Trop, L.; Hussey, D.; Singh, K.; Kung, H. F.; Kung, M. P.; Houle, S. *Am. J. Geriatr. Psychiatry* **2004**, *12*, 584.
9. Zhang, W.; Oya, S.; Kung, M. P.; Hou, C.; Maier, D. L.; Kung, H. F. *Nucl. Med. Biol.* **2005**, *32*, 799.
10. Rowe, C. C.; Ackerman, U.; Browne, W.; Mulligan, R.; Pike, K. L.; O'Keefe, G.; Tochon-Danguy, H.; Chan, G.; Berlangieri, S. U.; Jones, G.; Dickinson-Rowe, K. L.; Kung, H. P.; Zhang, W.; Kung, M. P.; Skovronsky, D.; Dyrks, T.; Holl, G.; Krause, S.; Friebe, M.; Lehman, L.; Lindemann, S.; Dinkelborg, L. M.; Masters, C. L.; Villemagne, V. L. *Lancet Neurol.* **2008**, *7*, 129.

11. Kudo, Y.; Okamura, N.; Furumoto, S.; Tashiro, M.; Furukawa, K.; Maruyama, M.; Itoh, M.; Iwata, R.; Yanai, K.; Arai, H. *J. Nucl. Med.* **2007**, *48*, 553.
12. Agdeppa, E. D.; Kepe, V.; Liu, J.; Flores-Torres, S.; Satyamurthy, N.; Petric, A.; Cole, G. M.; Small, G. W.; Huang, S. C.; Barrio, J. R. *J. Neurosci.* **2001**, *21*, RC189.
13. Shoghi-Jadid, K.; Small, G. W.; Agdeppa, E. D.; Kepe, V.; Ercoli, L. M.; Siddarth, P.; Read, S.; Satyamurthy, N.; Petric, A.; Huang, S. C.; Barrio, J. R. *Am. J. Geriatr. Psychiatry* **2002**, *10*, 24.
14. Kung, M. P.; Hou, C.; Zhuang, Z. P.; Zhang, B.; Skovronsky, D.; Trojanowski, J. Q.; Lee, V. M.; Kung, H. F. *Brain Res.* **2002**, *956*, 202.
15. Zhuang, Z. P.; Kung, M. P.; Wilson, A.; Lee, C. W.; Plossl, K.; Hou, C.; Holtzman, D. M.; Kung, H. F. *J. Med. Chem.* **2003**, *46*, 237.
16. Newberg, A. B.; Wintering, N. A.; Clark, C. M.; Plossl, K.; Skovronsky, D.; Seibyl, J. P.; Kung, M. P.; Kung, H. F. *J. Nucl. Med.* **2006**, *47*, 78P.
17. Zhang, W.; Kung, M. P.; Oya, S.; Hou, C.; Kung, H. F. *Nucl. Med. Biol.* **2007**, *34*, 89.
18. Choi, S. R.; Golding, G.; Zhuang, Z.; Zhang, W.; Lim, N.; Hefti, F.; Benedum, T. E.; Kilbourn, M. R.; Skovronsky, D.; Kung, H. F. *J. Nucl. Med.* **2009**, *50*, 1887.
19. Han, H.; Cho, C. G.; Lansbury, P. T., Jr. *J. Am. Chem. Soc.* **1996**, *118*, 4506.
20. Dezutter, N. A.; Dom, R. J.; de Groot, T. J.; Bormans, G. M.; Verbruggen, A. M. *Eur. J. Nucl. Med.* **1999**, *26*, 1392.
21. Chen, X.; Yu, P.; Zhang, L.; Liu, B. *Bioorg. Med. Chem. Lett.* **2008**, *18*, 1442.
22. Serdons, K.; Verduyckt, T.; Cleynhens, J.; Terwinghe, C.; Mortelmans, L.; Bormans, G.; Verbruggen, A. *Bioorg. Med. Chem. Lett.* **2007**, *17*, 6086.
23. Ono, M.; Yoshida, N.; Ishibashi, K.; Haratake, M.; Arano, Y.; Mori, H.; Nakayama, M. *J. Med. Chem.* **2005**, *48*, 7253.
24. Ono, M.; Haratake, M.; Mori, H.; Nakayama, M. *Bioorg. Med. Chem.* **2007**, *15*, 6802.
25. Ono, M.; Maya, Y.; Haratake, M.; Ito, K.; Mori, H.; Nakayama, M. *Biochem. Biophys. Res. Commun.* **2007**, *361*, 116.
26. Maya, Y.; Ono, M.; Watanabe, H.; Haratake, M.; Saji, H.; Nakayama, M. *Bioconjugate Chem.* **2009**, *20*, 95.
27. Ono, M.; Watanabe, R.; Kawashima, H.; Cheng, Y.; Kimura, H.; Watanabe, H.; Haratake, M.; Saji, H.; Nakayama, M. *J. Med. Chem.* **2009**, *52*, 6394.
28. Ono, M.; Watanabe, R.; Kawashima, H.; Kawai, T.; Watanabe, H.; Haratake, M.; Saji, H.; Nakayama, M. *Bioorg. Med. Chem.* **2009**, *17*, 2069.
29. Ono, M.; Ikeoka, R.; Watanabe, H.; Fuchigami, T.; Haratake, M.; Saji, H.; Nakayama, M. *ACS Chem. Neurosci.*, in press, doi:10.1021/cn100042d.
30. Oya, S.; Plossl, K.; Kung, M. P.; Stevenson, D. A.; Kung, H. F. *Nucl. Med. Biol.* **1998**, *25*, 135.

ACS Medicinal Chemistry Letters

pubs.acs.org/acsmedchemlett

Novel Benzofurans with ^{99m}Tc Complexes as Probes for Imaging Cerebral β-Amyloid Plaques

Masahiro Ono,*,†,‡ Yasufumi Fuchi,† Takeshi Fuchigami,† Nobuya Kobashi,† Hiroyuki Kimura,‡ Mamoru Haratake,† Hideo Saji,‡ and Morio Nakayama*,†

†Graduate School of Biomedical Sciences, Nagasaki University, 1-14 Bunkyo-machi, Nagasaki 852-8521, Japan, and ‡Graduate School of Pharmaceutical Sciences, Kyoto University, 46-29 Yoshida Shimoadachi-cho, Sakyo-ku, Kyoto 606-8501, Japan

ABSTRACT Two novel benzofuran derivatives coupled with ^{99m}Tc complexes were tested as probes for imaging cerebral β-amyloid plaques using single photon emission tomography. Although both derivatives bound to Aβ(1−42) aggregates, ^{99m}Tc-BAT-BF showed higher affinity than ^{99m}Tc-MAMA-BF. In sections of brain tissue from an animal model of AD, ^{99m}Tc-BAT-BF clearly labeled β-amyloid plaques. In biodistribution experiments using normal mice, ^{99m}Tc-BAT-BF displayed high uptake soon after its injection and washed out from the brain rapidly, a highly desirable feature for an imaging agent. ^{99m}Tc-BAT-BF may be a potential probe for imaging β-amyloid plaques in Alzheimer's brains.

KEYWORDS Alzheimer's disease, β-amyloid plaque, Tc-99m, single photon emission computed tomography (SPECT), imaging

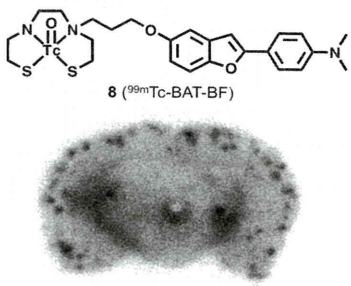

8 (^{99m}Tc-BAT-BF)

Alzheimer's disease (AD) is a neurodegenerative disease of the brain associated with irreversible cognitive decline, memory impairment, and behavioral changes. The presence of β-amyloid (Aβ) aggregates in the brain is generally accepted as a hallmark of AD.[1,2] Currently, the only definitive diagnosis of AD is by pathological examination of the postmortem staining of affected brain tissue, and the early appraisal of clinical symptoms for the diagnosis of AD is often difficult and unreliable. Thus, the detection of individual plaques in vivo by single photon emission tomography (SPECT) or positron emission tomography (PET) has been strongly desired to improve diagnosis and also accelerate the discovery of effective therapeutic agents for AD.[3−6] Many radiolabeled probes for imaging β-amyloid based on Congo Red, thioflavin T, and DDNP have been reported. Among them, [^{11}C]PIB,[7,8] [^{11}C]SB-13,[9,10] [^{18}F]BAY94-9172,[11,12] [^{11}C]BF-227,[13] [^{18}F]FDDNP,[14−16] [^{123}I]IMPY,[17−19] and [^{18}F]AV-45[20,21] have been tested clinically and demonstrated potential utility.

We have recently reported that ^{125}I-, ^{11}C-, and ^{18}F-labeled benzofuran derivatives showed high affinity for Aβ aggregates and good uptake into and rapid clearance from the brain, indicating that benzofuran can function as a promising scaffold for the development of β-amyloid imaging probes.[22,23] In this study, we planned the development of novel benzofuran derivatives labeled with technetium-99 m (^{99m}Tc). ^{99m}Tc ($T_{1/2}$ = 6.01 h, 141 keV) has become the most commonly used radionuclide in diagnostic nuclear medicine, because it is readily produced by an ^{99}Mo/^{99m}Tc generator; the medium γ-ray energy that it emits is suitable for detection, and its physical half-life is compatible with the biological localization and residence time required for imaging. Its ready availability, essentially 24 h a day, and easiness of use make it the radionuclide of choice. Several ^{99m}Tc-labeled imaging probes have been developed (Figure 1),[24−28] but no clinical study of them has been reported. New ^{99m}Tc-labeled imaging agents will provide simple, convenient, and widespread SPECT-based imaging methods for detecting and eventually quantifying β-amyloid plaques in living brain tissue.

In the present study, we synthesized two benzofuran derivatives with monoamine-monoamide dithiol (MAMA) and bis-amino-bis-thiol (BAT). MAMA and BAT were selected as a chelation ligand taking into consideration the permeability of the blood−brain barrier, because they form an electrically neutral complex with ^{99m}Tc.[29] We then evaluated their biological potential as probes by testing their affinity for Aβ aggregates and β-amyloid plaques in sections of brain tissue from Tg2576 mice and their uptake by and clearance from the brain in biodistribution experiments using normal mice. To our knowledge, this is the first time that benzofurans coupled with ^{99m}Tc complexes have been proposed as probes for the detection of β-amyloid plaques in the brain.

The synthesis of the ^{99m}Tc/Re benzofuran derivatives is outlined in Scheme 1. The key step in the formation of the benzofuran backbone was readily achieved by reacting 2-hydroxy-5-methoxybenzaldehyde with 4-nitrobenzylbromide to produce compound **1** in a yield of 75%. The amino derivative **2** was prepared from **1** by reduction with $SnCl_2$ in a yield of 95%.

Received Date: June 16, 2010
Accepted Date: July 26, 2010
Published on Web Date: August 02, 2010

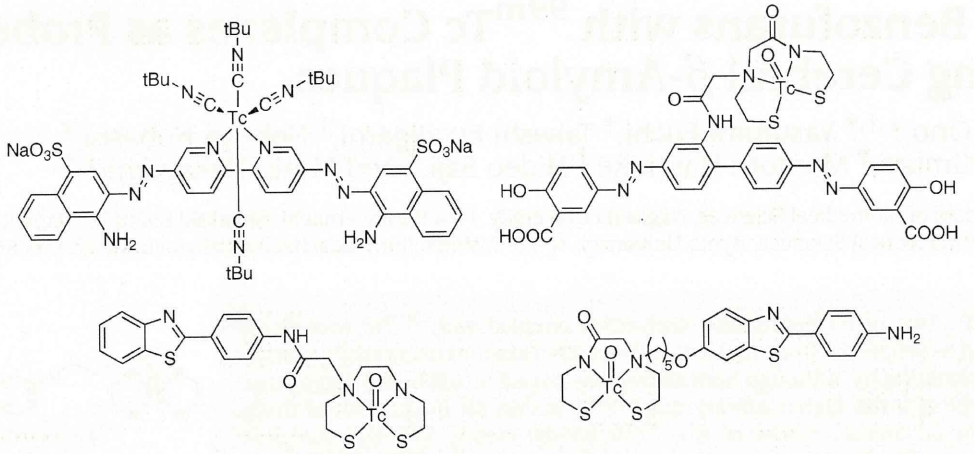

Figure 1. Chemical structure of ^{99m}Tc-labeled Aβ imaging probes reported previously.

Scheme 1. Synthesis of Re- and ^{99m}Tc-benzofuran Derivatives[a]

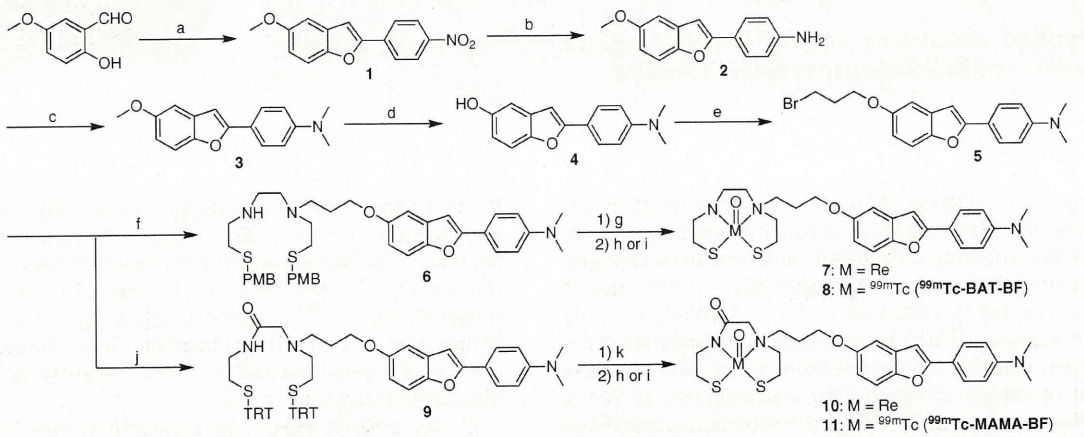

[a] Reagents: (a) DMF, K_2CO_3, 4-nitrobenzylbromide. (b) EtOH, $SnCl_2$. (c) CH_3COOH, $(CH_2O)_n$, $NaBH_3CN$. (d) CH_2Cl_2, BBr_3. (e) CH_3CN, K_2CO_3, 1,3-dibromopropane. (f) CH_3CN, DIPEA, PMB-BAT. (g) TFA, $MeSO_3H$, anisole. (h) CH_2Cl_2/MeOH, $(PPh_3)_2ReOCl_3$, AcONa. (i) CH_3CN, 0.1 N HCl, ^{99m}Tc-GH. (j) CH_3CN, TRT-MAMA, DIPEA. (k) TFA, Et_3SiH.

Conversion of **2** to the dimethylamino derivative **3** was achieved by an efficient method with paraformaldehyde, sodium cyanoborohydride, and acetic acid (78% yield). The *O*-methyl group of **3** was removed by reacting with BBr_3 to give **4** in a yield of 63%. After a trimethylene group was introduced into **4** as a linker by reacting with 1,3-dibromopropane, the chelation ligands were conjugated with **5**. The thiol-protected chelation ligands (PMB-BAT and TRT-MAMA) were synthesized according to methods reported previously with some slight modifications. Then, **5** was joined to PMB-BAT or TRT-MAMA to generate the compounds **6** (PMB-BAT-BF) and **9** (TRT-MAMA-BF), respectively. After deprotection of the thiol group in **6** and **9**, the Re complexes (**7** and **10**) were directly prepared by a reaction with $(PPh_3)_2ReOCl_3$. The corresponding ^{99m}Tc complex, **8** (^{99m}Tc-BAT-BF) or **11** (^{99m}Tc-MAMA-BF), was prepared by a ligand exchange reaction employing the precursor ^{99m}Tc-glucoheptonate (GH). The resulting mixture was analyzed by reversed-phase high-performance liquid chromatography (HPLC), showing that a single radioactive complex formed with radiochemical purity higher than 95% after purification by HPLC. The identity of the complex was established by comparative HPLC using the corresponding Re complexes as a reference. The retention times for ^{99m}Tc-BAT-BF and ^{99m}Tc-MAMA-BF on HPLC (radioactivity) were 13.2 and 10.3 min, respectively. The retention times of the corresponding Re complexes (**7** and **10**) on HPLC (UV detection) were 11.4 and 9.4 min, respectively.

To evaluate the binding affinity of Re-BAT-BF (**7**) and Re-MAMA-BF (**10**), inhibition assays with [^{125}I]IMPY and Aβ(1−42) aggregates were performed (Figure 2).[18] Both ligands inhibited the binding of [^{125}I]IMPY to Aβ(1−42) aggregates in a dose-dependent manner, indicating an affinity for Aβ aggregates. Their K_i values were 11.5 and 24.4 nM, respectively, suggesting that Re-BAT-BF displayed higher affinity than Re-MAMA-BF (Table 1). The results also indicated that ^{99m}Tc-BAT-BF and ^{99m}Tc-MAMA-BF would bind Aβ aggregates. Indeed, in subsequent assays, ^{99m}Tc-BAT-BF and ^{99m}Tc-MAMA-BF showed higher affinity than ^{99m}Tc-BAT and ^{99m}Tc-MAMA (Figure S1 in the Supporting Information). These results

DOI: 10.1021/ml100140d | ACS Med. Chem. Lett. 2010, 1, 443–447

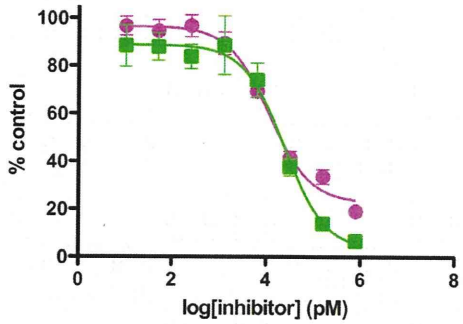

Figure 2. Inhibition curves of Re-BAT-BF (**7**) (pink circle) and Re-MAMA-BF (**10**) (green square) for the binding of [^{125}I]IMPY to Aβ(1−42) aggregates.

Table 1. Inhibition Constants for the Binding of [^{125}I]IMPY to Aβ(1−42) Aggregates

compound	K_i (nM)[a]
Re-BAT-BF (**7**)	11.5 ± 0.56
Re-MAMA-BF (**10**)	24.4 ± 0.77

[a] Values are the means ± standard errors of the mean of three independent determinations.

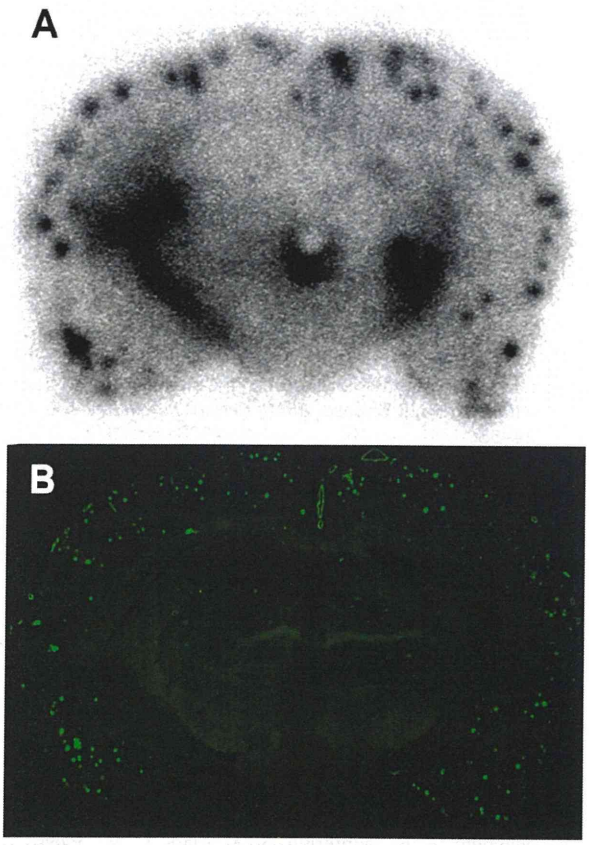

Figure 3. Autoradiography of ^{99m}Tc-BAT-BF in sections from Tg2576 mouse brain (A). Labeled plaques were confirmed by the staining of the adjacent sections with thioflavin-S (B).

strongly support our previous report that benzofuran derivatives have considerable tolerance for structural modifications.[22,23]

Next, the affinity of ^{99m}Tc-BAT-BF for β-amyloid plaques was investigated in vitro using sections of Tg2576 mouse brain (Figure 3). Autoradiographic images showed many radioactive spots in the brain tissue. Furthermore, the radioactivity of ^{99m}Tc-BAT-BF corresponded with the areas of staining with thioflavin-S, a pathological dye commonly used for β-amyloid plaques. In contrast, normal mouse brain displayed no remarkable accumulation of ^{99m}Tc-BAT-BF (data not shown). The results suggest that ^{99m}Tc-BAT-BF binds affinity for β-amyloid plaques in the mouse brain in addition to binding synthetic Aβ aggregates.

The biodistribution of ^{99m}Tc-BAT-BF and ^{99m}Tc-MAMA-BF was examined in normal mice (Table 2). A biodistribution experiment provides important information on uptake in the brain. The ideal imaging probe should penetrate the blood−brain barrier to deliver a sufficient dose into the brain but be rapidly cleared from normal regions so as to achieve in a high signal-to-noise ratio. ^{99m}Tc-BAT-BF showed greater uptake (1.34% ID/g) than ^{99m}Tc-MAMA-BF (0.74% ID/g) at 2 min postinjection. The uptake of ^{99m}Tc-BAT-BF peaked at 10 min postinjection, reaching 1.37% ID/g, and about 60% of radioactivity accumulated at 2 min postinjection had been washed out from the brain by 60 min. The uptake of

Table 2. Biodistribution of Radioactivity after Injection of ^{99m}Tc-Labeled Benzofuran Derivatives in Normal Mice[a]

	time after injection (min)			
organ	2	10	30	60
	^{99m}Tc-BAT-BF (**8**)			
blood	4.40 (0.27)	1.96 (0.06)	1.93 (0.26)	2.15 (0.91)
liver	21.94 (5.94)	20.87 (1.28)	19.65 (1.31)	15.09 (3.83)
kidney	10.28 (1.76)	7.90 (0.40)	4.27 (0.18)	2.70 (0.57)
intestine[b]	1.45 (0.18)	3.68 (0.52)	7.42 (1.62)	9.02 (1.93)
spleen	5.20 (1.01)	3.09 (0.23)	1.69 (0.21)	1.16 (0.14)
lung	26.70 (2.27)	6.48 (1.33)	3.51 (0.64)	2.36 (0.48)
stomach[b]	1.33 (0.57)	1.90 (0.43)	4.09 (1.37)	4.17 (1.92)
pancreas	4.14 (0.77)	4.57 (0.24)	2.98 (0.38)	1.42 (0.15)
heart	17.60 (2.60)	8.29 (0.97)	3.28 (1.35)	1.51 (0.25)
brain	1.34 (0.12)	1.37 (0.18)	0.94 (0.20)	0.56 (0.07)
	^{99m}Tc-MAMA-BF (**11**)			
blood	4.13 (0.42)	1.78 (0.25)	2.15 (0.12)	2.24 (0.24)
liver	20.17 (3.81)	21.62 (2.62)	23.32 (1.59)	20.16 (2.13)
kidney	7.37 (1.06)	8.09 (1.16)	5.11 (0.29)	3.28 (0.45)
intestine[b]	0.95 (0.22)	2.13 (0.19)	4.75 (0.93)	5.73 (0.66)
spleen	4.48 (0.56)	3.69 (0.34)	3.49 (0.61)	2.59 (0.65)
lung	24.04 (5.17)	7.59 (2.13)	4.24 (0.35)	3.54 (1.26)
stomach[b]	0.73 (0.21)	2.35 (0.58)	4.94 (0.57)	2.81 (0.51)
pancreas	2.70 (0.47)	4.00 (1.28)	5.48 (0.61)	3.76 (0.36)
heart	12.28 (2.20)	10.48 (1.79)	5.05 (0.90)	2.16 (0.34)
brain	0.74 (0.15)	0.99 (0.22)	1.23 (0.09)	0.89 (0.08)

[a] Each value represents the mean (SD) for five mice. Expressed as % injected dose per gram. [b] Expressed as % injected dose per organ.

DOI: 10.1021/ml100140d | ACS Med. Chem. Lett. 2010, 1, 443–447

^{99m}Tc-MAMA-BF peaked 30 min after the injection at 1.23% ID/g, and the washout from the brain was slower than that of ^{99m}Tc-BAT-BF throughout the time course, which is unsuitable for imaging in vivo. The log *P* values of ^{99m}Tc-BAT-BF and ^{99m}Tc-MAMA-BF were 3.33 and 3.01, respectively. Although lipophilicity is just one of the factors affecting the uptake of a compound into the brain,[4] it may explain the good uptake of ^{99m}Tc-BAT-BF.

In conclusion, we successfully designed and synthesized novel benzofuran derivatives conjugated with ^{99m}Tc or Re complexes for the detection of β-amyloid plaques in the brain. In experiments in vitro, Re-BAT-BF bound to Aβ aggregates with greater affinity than did Re-MAMA-BF, and ^{99m}Tc-BAT-BF clearly labeled β-amyloid plaques in sections of brain tissue from Tg2576 mice. In addition, ^{99m}Tc-BAT-BF displayed good uptake into and a rapid washout from the brain after its injection in normal mice. The combination of good affinity for β-amyloid plaques, uptake, and clearance makes ^{99m}Tc-BAT-BF a promising probe for the detection of β-amyloid plaques in the brain. The results of the present study should provide useful information for the development of ^{99m}Tc-labeled probes for the imaging of β-amyloid plaques in the brain.

SUPPORTING INFORMATION AVAILABLE

Procedures for the preparation of new ligands, analysis of data, experiments in vitro, and biodistribution experiments. This material is available free of charge via the Internet at http://pubs.acs.org.

AUTHOR INFORMATION

Corresponding Author: *To whom correspondence should be addressed. Tel: +81-75-753-4608. Fax: +81-75-753-4568. E-mail: ono@pharm.kyoto-u.ac.jp (M.O.). Tel: +81-95-819-2441. Fax: +81-95-819-2441. E-mail: morio@nagasaki-u.ac.jp (M.N.).

Funding Sources: This study was supported by Grants-in-Aid for Scientific Research (B), Young Scientists (A), and Exploratory Research from the Ministry of Education, Culture, Sports, Science and Technology, Japan.

REFERENCES

(1) Hardy, J. A.; Higgins, G. A. Alzheimer's disease: The amyloid cascade hypothesis. *Science* **1992,** *256*, 184–185.
(2) Selkoe, D. J. Alzheimer's disease: Genes, proteins, and therapy. *Physiol. Rev.* **2001,** *81*, 741–766.
(3) Selkoe, D. J. Imaging Alzheimer's amyloid. *Nat. Biotechnol.* **2000,** *18*, 823–824.
(4) Mathis, C. A.; Wang, Y.; Klunk, W. E. Imaging β-amyloid plaques and neurofibrillary tangles in the aging human brain. *Curr. Pharm. Des.* **2004,** *10*, 1469–1492.
(5) Nordberg, A. PET imaging of amyloid in Alzheimer's disease. *Lancet Neurol.* **2004,** *3*, 519–527.
(6) Kung, H. F.; Choi, S. R.; Qu, W.; Zhang, W.; Skovronsky, D. ^{18}F Stilbenes and Styrylpyridines for PET Imaging of Aβ Plaques in Alzheimer's Disease: A Miniperspective. *J. Med. Chem.* **2010,** *53*, 933–941.
(7) Mathis, C. A.; Wang, Y.; Holt, D. P.; Huang, G. F.; Debnath, M. L.; Klunk, W. E. Synthesis and evaluation of ^{11}C-labeled 6-substituted 2-arylbenzothiazoles as amyloid imaging agents. *J. Med. Chem.* **2003,** *46*, 2740–2754.
(8) Klunk, W. E.; Engler, H.; Nordberg, A.; Wang, Y.; Blomqvist, G.; Holt, D. P.; Bergstrom, M.; Savitcheva, I.; Huang, G. F.; Estrada, S.; Ausen, B.; Debnath, M. L.; Barletta, J.; Price, J. C.; Sandell, J.; Lopresti, B. J.; Wall, A.; Koivisto, P.; Antoni, G.; Mathis, C. A.; Langstrom, B. Imaging brain amyloid in Alzheimer's disease with Pittsburgh Compound-B. *Ann. Neurol.* **2004,** *55*, 306–319.
(9) Ono, M.; Wilson, A.; Nobrega, J.; Westaway, D.; Verhoeff, P.; Zhuang, Z. P.; Kung, M. P.; Kung, H. F. ^{11}C-labeled stilbene derivatives as Aβ-aggregate-specific PET imaging agents for Alzheimer's disease. *Nucl. Med. Biol.* **2003,** *30*, 565–571.
(10) Verhoeff, N. P.; Wilson, A. A.; Takeshita, S.; Trop, L.; Hussey, D.; Singh, K.; Kung, H. F.; Kung, M. P.; Houle, S. In-vivo imaging of Alzheimer disease β-amyloid with [^{11}C]SB-13 PET. *Am. J. Geriatr. Psychiatry* **2004,** *12*, 584–595.
(11) Zhang, W.; Oya, S.; Kung, M. P.; Hou, C.; Maier, D. L.; Kung, H. F. F-18 polyethyleneglycol stilbenes as PET imaging agents targeting Aβ aggregates in the brain. *Nucl. Med. Biol.* **2005,** *32*, 799–809.
(12) Rowe, C. C.; Ackerman, U.; Browne, W.; Mulligan, R.; Pike, K. L.; O'Keefe, G.; Tochon-Danguy, H.; Chan, G.; Berlangieri, S. U.; Jones, G.; Dickinson-Rowe, K. L.; Kung, H. P.; Zhang, W.; Kung, M. P.; Skovronsky, D.; Dyrks, T.; Holl, G.; Krause, S.; Friebe, M.; Lehman, L.; Lindemann, S.; Dinkelborg, L. M.; Masters, C. L.; Villemagne, V. L. Imaging of amyloid β in Alzheimer's disease with ^{18}F-BAY94-9172, a novel PET tracer: Proof of mechanism. *Lancet Neurol.* **2008,** *7*, 129–135.
(13) Kudo, Y.; Okamura, N.; Furumoto, S.; Tashiro, M.; Furukawa, K.; Maruyama, M.; Itoh, M.; Iwata, R.; Yanai, K.; Arai, H. 2-(2-[2-Dimethylaminothiazol-5-yl]ethenyl)-6-(2-[fluoro]ethoxy)-benzoxazole: A novel PET agent for in vivo detection of dense amyloid plaques in Alzheimer's disease patients. *J. Nucl. Med.* **2007,** *48*, 553–561.
(14) Agdeppa, E. D.; Kepe, V.; Liu, J.; Flores-Torres, S.; Satyamurthy, N.; Petric, A.; Cole, G. M.; Small, G. W.; Huang, S. C.; Barrio, J. R. Binding characteristics of radiofluorinated 6-dialkylamino-2-naphthylethylidene derivatives as positron emission tomography imaging probes for β-amyloid plaques in Alzheimer's disease. *J. Neurosci.* **2001,** *21*, RC189.
(15) Shoghi-Jadid, K.; Small, G. W.; Agdeppa, E. D.; Kepe, V.; Ercoli, L. M.; Siddarth, P.; Read, S.; Satyamurthy, N.; Petric, A.; Huang, S. C.; Barrio, J. R. Localization of neurofibrillary tangles and β-amyloid plaques in the brains of living patients with Alzheimer disease. *Am. J. Geriatr. Psychiatry* **2002,** *10*, 24–35.
(16) Small, G. W.; Kepe, V.; Ercoli, L. M.; Siddarth, P.; Bookheimer, S. Y.; Miller, K. J.; Lavretsky, H.; Burggren, A. C.; Cole, G. M.; Vinters, H. V.; Thompson, P. M.; Huang, S. C.; Satyamurthy, N.; Phelps, M. E.; Barrio, J. R. PET of brain amyloid and tau in mild cognitive impairment. *N. Engl. J. Med.* **2006,** *355*, 2652–2663.
(17) Kung, M. P.; Hou, C.; Zhuang, Z. P.; Zhang, B.; Skovronsky, D.; Trojanowski, J. Q.; Lee, V. M.; Kung, H. F. IMPY: An improved thioflavin-T derivative for *in vivo* labeling of β-amyloid plaques. *Brain Res.* **2002,** *956*, 202–210.
(18) Zhuang, Z. P.; Kung, M. P.; Wilson, A.; Lee, C. W.; Plossl, K.; Hou, C.; Holtzman, D. M.; Kung, H. F. Structure-activity relationship of imidazo[1,2-a]pyridines as ligands for detecting β-amyloid plaques in the brain. *J. Med. Chem.* **2003,** *46*, 237–243.
(19) Newberg, A. B.; Wintering, N. A.; Clark, C. M.; Plossl, K.; Skovronsky, D.; Seibyl, J. P.; Kung, M. P.; Kung, H. F. Use of ^{123}I IMPY SPECT to differentiate Alzheimer's disease from controls. *J. Nucl. Med.* **2006,** *47*, 78P.

(20) Zhang, W.; Kung, M. P.; Oya, S.; Hou, C.; Kung, H. F. ^{18}F-labeled styrylpyridines as PETagents for amyloid plaque imaging. *Nucl. Med. Biol.* **2007,** *34*, 89–97.
(21) Choi, S. R.; Golding, G.; Zhuang, Z.; Zhang, W.; Lim, N.; Hefti, F.; Benedum, T. E.; Kilbourn, M. R.; Skovronsky, D.; Kung, H. F. Preclinical properties of ^{18}F-AV-45: A PET agent for Aβ plaques in the brain. *J. Nucl. Med.* **2009,** *50*, 1887–1894.
(22) Ono, M.; Kung, M. P.; Hou, C.; Kung, H. F. Benzofuran derivatives as Aβ-aggregate-specific imaging agents for Alzheimer's disease. *Nucl. Med. Biol.* **2002,** *29*, 633–642.
(23) Ono, M.; Kawashima, H.; Nonaka, A.; Kawai, T.; Haratake, M.; Mori, H.; Kung, M. P.; Kung, H. F.; Saji, H.; Nakayama, M. Novel benzofuran derivatives for PET imaging of β-amyloid plaques in Alzheimer's disease brains. *J. Med. Chem.* **2006,** *49*, 2725–2730.
(24) Han, H.; Cho, C. G.; Lansbury, P. T., Jr. Technetium complexes for the quantitation of brain amyloid. *J. Am. Chem. Soc.* **1996,** *118*, 4506–4507.
(25) Dezutter, N. A.; Dom, R. J.; de Groot, T. J.; Bormans, G. M.; Verbruggen, A. M. ^{99m}Tc-MAMA-chrysamine G, a probe for β-amyloid protein of Alzheimer's disease. *Eur. J. Nucl. Med.* **1999,** *26*, 1392–1399.
(26) Chen, X.; Yu, P.; Zhang, L.; Liu, B. Synthesis and biological evaluation of ^{99m}Tc, Re-monoamine-monoamide conjugated to 2-(4-aminophenyl)benzothiazole as potential probes for β-amyloid plaques in the brain. *Bioorg. Med. Chem. Lett.* **2008,** *18*, 1442–1445.
(27) Serdons, K.; Verduyckt, T.; Cleynhens, J.; Terwinghe, C.; Mortelmans, L.; Bormans, G.; Verbruggen, A. Synthesis and evaluation of a ^{99m}Tc-BAT-phenylbenzothiazole conjugate as a potential in vivo tracer for visualization of amyloid β. *Bioorg. Med. Chem. Lett.* **2007,** *17*, 6086–6090.
(28) Zhuang, Z. P.; Kung, M. P.; Hou, C.; Ploessl, K.; Kung, H. F. Biphenyls labeled with technetium 99m for imaging β-amyloid plaques in the brain. *Nucl. Med. Biol.* **2005,** *32*, 171–184.
(29) Oya, S.; Plossl, K.; Kung, M. P.; Stevenson, D. A.; Kung, H. F. Small and neutral Tc(v)O BAT, bisaminoethanethiol (N_2S_2) complexes for developing new brain imaging agents. *Nucl. Med. Biol.* **1998,** *25*, 135–140.

DOI: 10.1021/ml100140d | *ACS Med. Chem. Lett.* **2010,** *1*, 443–447

Bioorganic & Medicinal Chemistry Letters 20 (2010) 6141–6144

Contents lists available at ScienceDirect

Bioorganic & Medicinal Chemistry Letters

journal homepage: www.elsevier.com/locate/bmcl

A novel ^{18}F-labeled pyridyl benzofuran derivative for imaging of β-amyloid plaques in Alzheimer's brains

Yan Cheng [a], Masahiro Ono [a,*], Hiroyuki Kimura [a], Shinya Kagawa [b], Ryuichi Nishii [b], Hideo Saji [a,*]

[a] Graduate School of Pharmaceutical Sciences, Kyoto University, 46-29 Yoshida Shimoadachi-cho, Sakyo-ku, Kyoto 606-8501, Japan
[b] Shiga Medical Center Research Institute, 5-4-30, Moriyama, Moriyama City, Shiga 524-8524, Japan

ARTICLE INFO

Article history:
Received 20 May 2010
Revised 22 July 2010
Accepted 4 August 2010
Available online 8 August 2010

Keywords:
Alzheimer's disease
β-Amyloid plaques
Positron emission tomography (PET)
Benzofuran

ABSTRACT

A potential probe for PET targeting β-amyloid plaques in Alzheimer's disease (AD) brain, FPYBF-1 (5-(5-(2-(2-(2-fluoroethoxy)ethoxy)ethoxy)benzofuran-2-yl)-*N*,*N*-dimethylpyridin-2-amine), was synthesized and evaluated. In experiments in vitro, FPYBF-1 displayed high affinity for Aβ(1–42) aggregates (K_i = 0.9 nM), and substantial labeling of β-amyloid plaques in sections of postmortem AD brains but not control brains. In experiments in vivo, [^{18}F]FPYBF-1 displayed good initial uptake (5.16%ID/g at 2 min postinjection) and rapid washout from the brain (2.44%ID/g at 60 min postinjection) in normal mice, and excellent binding to β-amyloid plaques in a murine model of AD. Furthermore, the specific labeling of plaques labeling was observed in autoradiographs of autopsied AD brain sections. [^{18}F]FPYBF-1 may be a useful probe for imaging β-amyloid plaques in living brain tissue.

Alzheimer's disease (AD) is a progressive neurodegenerative disorder characterized by cognitive decline, irreversible memory loss, disorientation, and language impairment. The presence of β-amyloid (Aβ) aggregates in the brain is generally accepted as a hallmark of AD.[1,2] Since the only definitive diagnosis of AD is by pathological examination of autopsied brain tissue, the development of techniques which enable the imaging of β-amyloid plaques in vivo has been strongly desired.[3–5]

Preliminary studies with positron emission tomography (PET) suggested that [^{11}C]4-*N*-methylamino-4′-hydroxystilbene (SB-13),[6,7] [^{11}C] 2-(4′-(methylaminophenyl)-6-hydroxybenzothiazole (PIB),[8,9] [^{11}C]2-(2-[2-dimethylaminothiazol-5-yl]ethenyl)-6-(2-[fluoro]ethoxy)benzoxazole (BF-227),[10] and [^{11}C]-2-[6-(methylamino)pyridin-3-yl]-1,3-benzothiazol-6-ol (AZD2184)[11] differed in their uptake and retention in the brain between AD patients and controls (Fig. 1). Success in using ^{11}C-labeled tracers to image β-amyloid plaques in the brain in cases of suspected AD has provided considerable impetus for further refinement of this technique. However, the short half-life of ^{11}C ($t_{1/2}$: 20 min) limits its potential as a diagnostic tool. Since ^{18}F with a longer half-life isotope ($t_{1/2}$: 110 min) would be more useful for this purpose, recent efforts have focused on the development of comparable agents labeled with ^{18}F. Preliminary studies with [^{18}F]-2-(1-(2-(*N*-(2-fluoroethyl)-*N*-methylamino)naphthalene-6-yl)ethylidene)malononitrile (FDDNP)[12,13] showed differential uptake and retention in the brain of AD patients for the first time. More recently, a stilbene derivative, (*E*)-4-(*N*-methylamino)-4′-(2-(2-(2-[^{18}F]-fluoroethoxy)ethoxy)-ethoxy)-stilbene (BAY94-9172),[14,15] a styryl pyridine derivative, (*E*)-4-(2-(6-(2-(2-(2-([^{18}F]-fluoroethoxy)ethoxy)ethoxy)pyridyn-3-ylvinyl)-*N*-methyl benzenamine (AV-45),[16–18] and a PIB analogue, 2-(3-[^{18}F]-fluoro-4-methyamino-phenyl)benzothiazol-6-ol (GE-067),[19] have been shown to be useful for the imaging of β-amyloid plaques in living brain tissue in phase II or III clinical trials (Fig. 1).[20]

We have evaluated a series of fluorinated benzofuran derivatives as potential ^{18}F-labeled tracers for the imaging of β-amyloid plaques by PET.[21] These derivatives displayed excellent affinity for Aβ aggregates in vitro and in vivo. The penetration of brain tissues by 4-(5-(2-(2-(2-fluoroethoxy)ethoxy)ethoxy)benzofuran-2-yl)-*N*,*N*-dimethylbenzenamine (FPHBF-1, Fig. 2) was particularly encouraging. However, the slow washout of this probe from the normal mouse brain made it unsuitable for imaging in vivo. Therefore, a critical need to fine-tune the kinetics of the uptake and washout of benzofuran derivatives exists. Previous results regarding uptake into and clearance from the brain point to high lipophilicity as one of the reasons for a slow washout from the brain.[8,22–24]

We planned to develop a novel fluorinated pyridyl benzofuran derivative with less lipophilicity by displacing of the phenyl group in phenyl benzofuran with a pyridyl group. Kung and co-workers exploited a novel approach, fluoro-pegylation (FPEG) of the core structure, to label derivatives with ^{18}F.[25] Since this approach offers

* Corresponding authors. Tel.: +81 75 753 4608; fax: +81 75 753 4568 (M.O.); tel.: +81 75 753 4556; fax: +81 75 753 4568 (H.S.).
E-mail addresses: ono@pharm.kyoto-u.ac.jp (M. Ono), hsaji@pharm.kyoto-u.ac.jp (H. Saji).

0960-894X/$ - see front matter © 2010 Elsevier Ltd. All rights reserved.
doi:10.1016/j.bmcl.2010.08.016

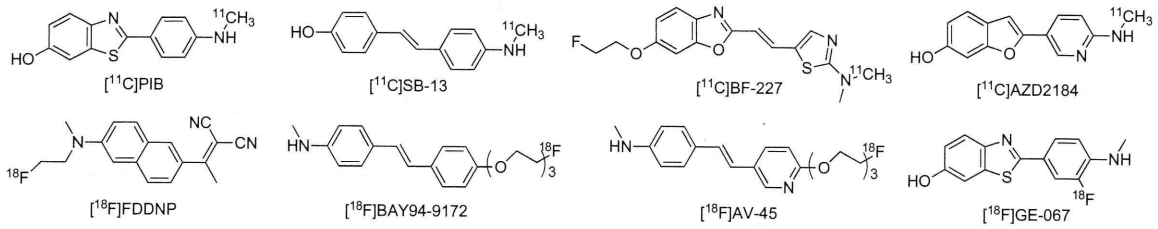

Figure 1. Chemical structure of PET imaging agents targeting β-amyloid plaques in AD patients.

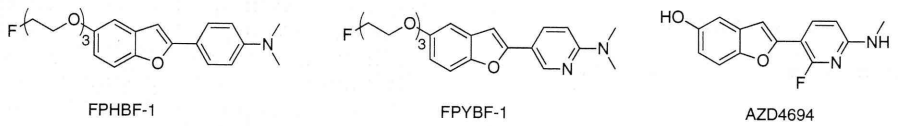

Figure 2. Chemical structure of benzofuran derivatives, FPHBF-1, FPYBF-1, and AZD4694.

a simple and easy way to incorporate ^{18}F into a target without an appreciable increase in lipophilicity, we selected FPEG for the labeling of pyridyl benzofuran derivatives. We designed a novel fluorinated ligand, 5-(5-(2-(2-(2-fluoroethoxy)ethoxy)ethoxy)benzofuran-2-yl)-*N*,*N*-dimethylpyridin-2-amine (FPYBF-1, Fig. 2) with a fluoropolyethylene glycol side chain and a dimethylamino pyridyl group. Another group recently reported a different fluorinated pyridyl benzofuran derivative, 2-(2-fluoro-6-(methylamino)pyridin-3-yl)benzofuran-5-ol (AZD4694, Fig. 2) to have potential for the imaging of cerebral β-amyloid plaques in living brain tissue.[26] However, they did not report the ^{18}F-labeling or in vivo characteristics of [^{18}F]AZD4694. This is the first time that a pyridyl benzofuran derivative has been successfully radiolabeled with ^{18}F and evaluated for the imaging of β-amyloid plaques in vivo.

The synthesis of **5** (FPYBF-1) is outlined in Scheme 1. The key step in the formation of the pyridyl benzofuran backbone is accomplished by Suzuki coupling between 5-methoxybenzofuran-2-boronic acid and 2-amino-5-iodopyridine.[27] Suzuki coupling afforded the desired compound **1** in a yield of 52.1%. Conversion of **1** to the corresponding dimethylamino derivative **2** was achieved by dimethylation with paraformaldehyde and sodium cyanoborohydride (yield 62%). A methoxy group of **2** was converted to a hydroxyl group using BBr_3/CH_2Cl_2, which afforded **3** in a yield of 98.9%. The synthesis of **4**–**6** was achieved using conventional methods reported previously.[28] The ^{18}F-labeled **5** ([^{18}F]FPYBF-1) was prepared from a tosyl precursor (**6**) via a nucleophilic displacement reaction with a fluoride anion as shown in Scheme 2. Radiolabeling of the precursor generated [^{18}F]FPYBF-1 with an average radiochemical yield of 52% and radiochemical purity of >99%, and a specific activity of 242 GBq/μmol. The identity of [^{18}F]FPYBF-1 was verified by a comparison of the retention time with the nonradioactive compound.

Experiments in vitro to evaluate the affinity of FPYBF-1 for Aβ aggregates were carried out in solutions with [^{125}I]IMPY as the ligand according to conventional methods.[29,30] FPYBF-1 inhibited the binding of [^{125}I]IMPY in a dose-dependent manner with a K_i value of 0.9 nM, indicating that it has excellent affinity for Aβ(1–42) aggregates (Fig. 3). This K_i value is similar to that of phenyl benzofuran derivatives (K_i = 2.0 nM) reported previously,[21] and the affinity of the pyridyl benzofuran derivative for Aβ(1–42) aggregates remained high despite displacement of the phenyl group with a pyridyl group. This result also shows that the benzofuran scaffold can tolerate extensive structural modification.[21,22,31]

To evaluate the uptake of [^{18}F]FPYBF-1 in the brain, a biodistribution experiment was performed in normal mice (Table 1).

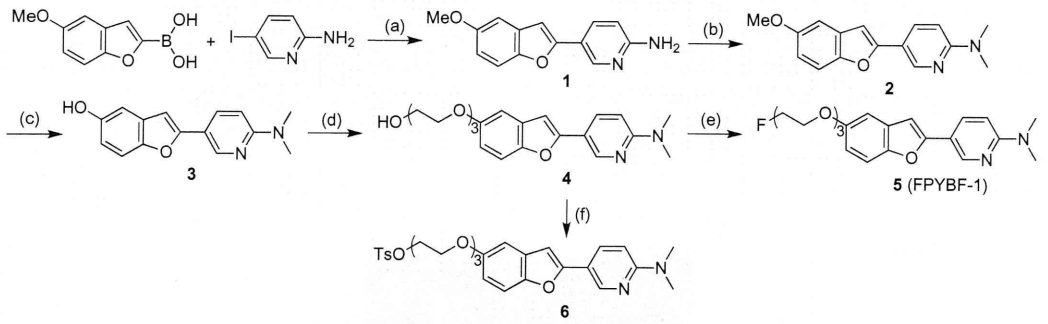

Scheme 1. Reagents and conditions: (a) $Pd(Ph_3P)_4$, Na_2CO_3 (aq)/dioxane, reflux.; (b) paraformaldehyde, sodium cyanoborohydride, acetic acid, rt; (c)BBr_3, CH_2Cl_2, rt; (d) 2-[2-(2-chloroethoxy)ethoxy]ethanol, K_2CO_3, DMF, 100 °C; (e) DAST, DME, 0 °C; (f) tosyl chloride, pyridine, rt.

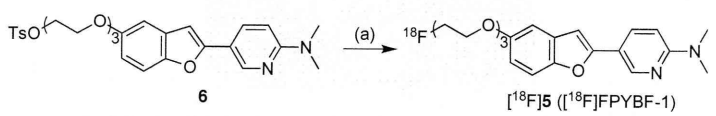

Scheme 2. Reagents and conditions: (a) Kryptofix222, K_2CO_3, acetonitrile, 120 °C.

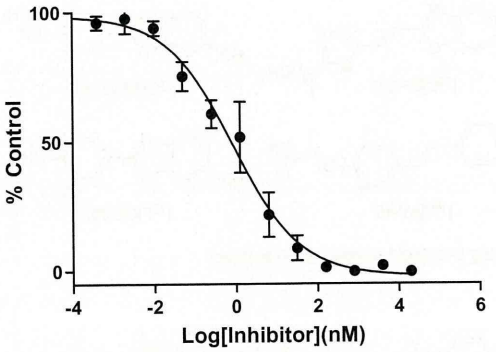

Figure 3. Competition curve of FPYBF-1 against [^{125}I]IMPY.

[^{18}F]FPYBF-1 displayed high uptake (5.16%ID/g) at 2 min postinjection, sufficient for PET, and the radioactivity in the brain cleared with time (2.44%ID/g at 60 min postinjection). Since normal brain tissue has no β-amyloid plaques to trap [^{18}F]FPYBF-1, the radioactivity should wash out quite rapidly. Therefore, the rapid clearance of [^{18}F]FPYBF-1 from normal brain is appropriate for the detection of β-amyloid plaques in the AD brain. One way to select a ligand with appropriate kinetics in vivo is to use the $brain_{2\ min}/brain_{60\ min}$ ratio as an index to compare the washout rate.[32] Although the $brain_{2\ min}/brain_{60\ min}$ ratio of [^{18}F]FPYBF-1 (2.1) was lower than that of [^{18}F]BAY94-9172 (4.8)[14] or [^{18}F]AV-45 (3.8),[16] it was improved as compared to the values for [^{18}F]FPHBF-1 (1.0) reported previously.[21] The favorable in vivo pharmacokinetics of [^{18}F]FPYBF-1 were achieved by changing the phenyl group in [^{18}F]FPHBF-1 to a pyridyl group. In HPLC analyses, [^{18}F]FPYBF-1 and [^{18}F]FPHBF-1 showed retention times of 14.8 and 36.5 min, respectively, indicating that [^{18}F]FPYBF-1 is less lipophilic than [^{18}F]FPHBF-1. Although lipophil-

Table 1
Biodistribution of radioactivity after injection of [^{18}F]FPYBF-1 in normal mice[a]

Organ	2 min	10 min	30 min	60 min
Blood	2.83 ± 0.89	2.13 ± 0.49	1.76 ± 0.09	1.98 ± 0.35
Brain	5.16 ± 0.30	3.75 ± 0.64	2.78 ± 0.22	2.44 ± 0.36
Bone	1.61 ± 0.33	1.33 ± 0.28	1.11 ± 0.13	1.42 ± 0.24

[a] Expressed as % of injected dose per gram. Each value represents the mean ± SD for five mice.

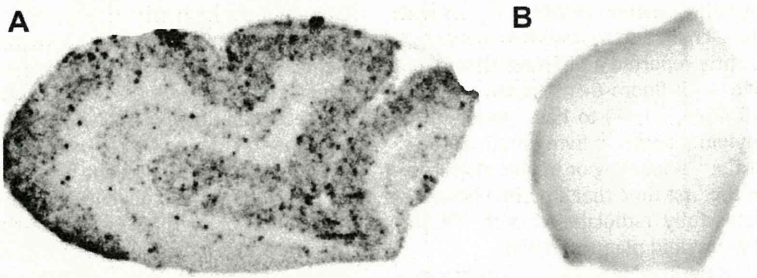

Figure 4. In vitro autoradiograms of sections of AD brain labeled with [^{18}F]FPYBF-1. Intensive labeling of β-amyloid plaques in brain tissue from AD patients (A). The control subject exhibits no labeling by this tracer (B).

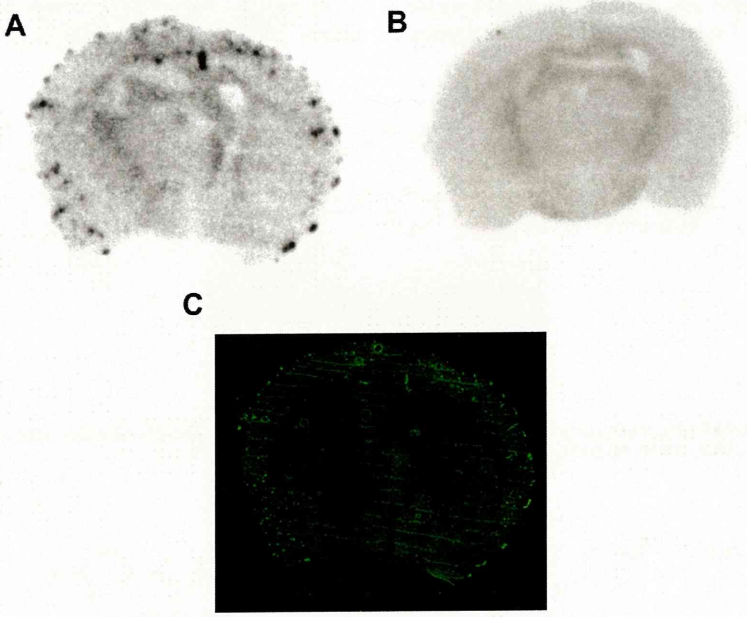

Figure 5. The labeling of β-amyloid plaques in vivo was visualized by autoradiography ex vivo with [^{18}F]FPYBF-1 in sections of Tg2576 mouse brain (A). The same section was also stained with thioflavin-S (C). Wild-type mouse brain showed no β-amyloid plaques (B).

icity is just one of the factors affecting the uptake of a compound into the brain,[4] it may explain the favorable pharmacokinetics of [^{18}F]FPYBF-1 in the brain. Uptake in the bone at 60 min was reduced (1.42%ID/g), suggesting little defluorination in vivo and interference with the imaging is expected to be relatively minor.

Next, sections of brain tissue from AD and control subjects (5 μm) were used to confirm the specific binding of [^{18}F]FPYBF-1 to β-amyloid plaques. Autoradiographic images revealed extensive labeling of β-amyloid plaques in the AD brain (Fig. 4A) but not control brain (Fig. 4B). The results suggest that [^{18}F]FPYBF-1 shows affinity for β-amyloid plaques in addition to synthetic Aβ aggregates.

To further characterize the potential of [^{18}F]FPYBF-1 as a probe for imaging β-amyloid plaques in living brain tissue, we carried out autoradiography ex vivo in Tg2576 mice (36 months, male) and in wild-type mice (36 months, male) as age-matched controls. Tg2576 transgenic mice show marked Aβ deposition in the cingulated cortex, entorhinal cortex, dentate gyrus, and CA1 hippocampal subfield by 11–13 months of age[33] and have been frequently used to evaluate the specific binding of β-amyloid plaques in experiments in vitro and in vivo.[28,34,35] The autoradiography showed clear labeling of β-amyloid plaques in the Tg2576 mouse brain (Fig. 5A). Wild-type mouse brain showed no such labeling (Fig. 5B). β-Amyloid plaques were confirmed present by co-staining the sections with thioflavin-S, a pathological dye commonly used to stain β-amyloid plaques (Fig. 5C). This is consistent with the results in vitro, showing [^{18}F]FPYBF-1 to be highly selective in binding to β-amyloid plaques in the brain.

In conclusion, based on previous results, we designed a novel fluorinated pyridyl benzofuran ligand, FPYBF-1, for the imaging of β-amyloid plaques in the brain. FPYBF-1 showed high binding affinity for Aβ aggregates in vitro and for β-amyloid plaques in sections of autopsied AD brain. It also displayed good uptake in the brain (5.16%ID/g at 2 min postinjection) and excellent binding to β-amyloid plaques ex vivo in transgenic mice. [^{18}F]FPYBF-1 is now under preclinical evaluation for use as a probe in PET. Other pyridyl benzofuran derivatives are also under investigation.

Acknowledgments

The study was supported by a Grant-in-aid for Young Scientists (A) and Exploratory Research from the Ministry of Education, Culture, Sports, Science and Technology.

Supplementary data

Supplementary data associated with this article can be found, in the online version, at doi:10.1016/j.bmcl.2010.08.016.

References and notes

1. Hardy, J. A.; Higgins, G. A. *Science* **1992**, *256*, 184.
2. Selkoe, D. J. *Physiol. Rev.* **2001**, *81*, 741.
3. Selkoe, D. J. *Nat. Biotechnol.* **2000**, *18*, 823.
4. Mathis, C. A.; Wang, Y.; Klunk, W. E. *Curr. Pharm. Des.* **2004**, *10*, 1469.
5. Nordberg, A. *Lancet Neurol.* **2004**, *3*, 519.
6. Ono, M.; Wilson, A.; Nobrega, J.; Westaway, D.; Verhoeff, P.; Zhuang, Z. P.; Kung, M. P.; Kung, H. F. *Nucl. Med. Biol.* **2003**, *30*, 565.
7. Verhoeff, N. P.; Wilson, A. A.; Takeshita, S.; Trop, L.; Hussey, D.; Singh, K.; Kung, H. F.; Kung, M. P.; Houle, S. *Am. J. Geriatr. Psychiatry* **2004**, *12*, 584.
8. Mathis, C. A.; Wang, Y.; Holt, D. P.; Huang, G. F.; Debnath, M. L.; Klunk, W. E. *J. Med. Chem.* **2003**, *46*, 2740.
9. Klunk, W. E.; Engler, H.; Nordberg, A.; Wang, Y.; Blomqvist, G.; Holt, D. P.; Bergstrom, M.; Savitcheva, I.; Huang, G. F.; Estrada, S.; Ausen, B.; Debnath, M. L.; Barletta, J.; Price, J. C.; Sandell, J.; Lopresti, B. J.; Wall, A.; Koivisto, P.; Antoni, G.; Mathis, C. A.; Langstrom, B. *Ann. Neurol.* **2004**, *55*, 306.
10. Kudo, Y.; Okamura, N.; Furumoto, S.; Tashiro, M.; Furukawa, K.; Maruyama, M.; Itoh, M.; Iwata, R.; Yanai, K.; Arai, H. *J. Nucl. Med.* **2007**, *48*, 553.
11. Johnson, A. E.; Jeppsson, F.; Sandell, J.; Wensbo, D.; Neelissen, J. A.; Jureus, A.; Strom, P.; Norman, H.; Farde, L.; Svensson, S. P. *J. Neurochem.* **2009**, *108*, 1177.
12. Agdeppa, E. D.; Kepe, V.; Liu, J.; Flores-Torres, S.; Satyamurthy, N.; Petric, A.; Cole, G. M.; Small, G. W.; Huang, S. C.; Barrio, J. R. *J. Neurosci.* **2001**, *21*, RC189.
13. Shoghi-Jadid, K.; Small, G. W.; Agdeppa, E. D.; Kepe, V.; Ercoli, L. M.; Siddarth, P.; Read, S.; Satyamurthy, N.; Petric, A.; Huang, S. C.; Barrio, J. R. *Am. J. Geriatr. Psychiatry* **2002**, *10*, 24.
14. Zhang, W.; Oya, S.; Kung, M. P.; Hou, C.; Maier, D. L.; Kung, H. F. *Nucl. Med. Biol.* **2005**, *32*, 799.
15. Rowe, C. C.; Ackerman, U.; Browne, W.; Mulligan, R.; Pike, K. L.; O'Keefe, G.; Tochon-Danguy, H.; Chan, G.; Berlangieri, S. U.; Jones, G.; Dickinson-Rowe, K. L.; Kung, H. P.; Zhang, W.; Kung, M. P.; Skovronsky, D.; Dyrks, T.; Holl, G.; Krause, S.; Friebe, M.; Lehman, L.; Lindemann, S.; Dinkelborg, L. M.; Masters, C. L.; Villemagne, V. L. *Lancet Neurol.* **2008**, *7*, 129.
16. Zhang, W.; Kung, M. P.; Oya, S.; Hou, C.; Kung, H. F. *Nucl. Med. Biol.* **2007**, *34*, 89.
17. Choi, S. R.; Golding, G.; Zhuang, Z.; Zhang, W.; Lim, N.; Hefti, F.; Benedum, T. E.; Kilbourn, M. R.; Skovronsky, D.; Kung, H. F. *J. Nucl. Med.* **2009**, *50*, 1887.
18. Wong, D. F.; Rosenberg, P. B.; Zhou, Y.; Kumar, A.; Raymont, V.; Ravert, H. T.; Dannals, R. F.; Nandi, A.; Brasic, J. R.; Ye, W.; Hilton, J.; Lyketsos, C.; Kung, H. F.; Joshi, A. D.; Skovronsky, D. M.; Pontecorvo, M. J. *J. Nucl. Med.* **2010**, *51*, 913.
19. Koole, M.; Lewis, D. M.; Buckley, C.; Nelissen, N.; Vandenbulcke, M.; Brooks, D. J.; Vandenberghe, R.; Van Laere, K. *J. Nucl. Med.* **2009**, *50*, 818.
20. Kung, H. F.; Choi, S. R.; Qu, W.; Zhang, W.; Skovronsky, D. *J. Med. Chem.* **2010**, *53*, 933.
21. Cheng, Y.; Ono, M.; Kimura, H.; Kagawa, S.; Nishii, R.; Kawashima, H.; Saji, H. *ACS Med. Chem. Lett.* in press, doi:10.1021/ml100082x.
22. Ono, M.; Kawashima, H.; Nonaka, A.; Kawai, T.; Haratake, M.; Mori, H.; Kung, M. P.; Kung, H. F.; Saji, H.; Nakayama, M. *J. Med. Chem.* **2006**, *49*, 2725.
23. Ono, M.; Yoshida, N.; Ishibashi, K.; Haratake, M.; Arano, Y.; Mori, H.; Nakayama, M. *J. Med. Chem.* **2005**, *48*, 7253.
24. Ono, M.; Haratake, M.; Mori, H.; Nakayama, M. *Bioorg. Med. Chem.* **2007**, *15*, 6802.
25. Stephenson, K. A.; Chandra, R.; Zhuang, Z. P.; Hou, C.; Oya, S.; Kung, M. P.; Kung, H. F. *Bioconjugate Chem.* **2007**, *18*, 238.
26. Jureus, A.; Swahn, B. M.; Sandell, J.; Jeppsson, F.; Johnson, A. E.; Johnstrom, P.; Neelissen, J. A.; Sunnemark, D.; Farde, L.; Svensson, S. P. *J. Neurochem.* **2010**.
27. Miyaura, N.; Yamada, K.; Suzuki, A. *Tetrahedron Lett.* **1979**, *36*, 3437.
28. Ono, M.; Watanabe, R.; Kawashima, H.; Cheng, Y.; Kimura, H.; Watanabe, H.; Haratake, M.; Saji, H.; Nakayama, M. *J. Med. Chem.* **2009**, *52*, 6394.
29. Ono, M.; Haratake, M.; Saji, H.; Nakayama, M. *Bioorg. Med. Chem.* **2008**, *16*, 6867.
30. Watanabe, H.; Ono, M.; Ikeoka, R.; Haratake, M.; Saji, H.; Nakayama, M. *Bioorg. Med. Chem.* **2009**, *17*, 6402.
31. Ono, M.; Kung, M. P.; Hou, C.; Kung, H. F. *Nucl. Med. Biol.* **2002**, *29*, 633.
32. Maya, Y.; Ono, M.; Watanabe, H.; Haratake, M.; Saji, H.; Nakayama, M. *Bioconjugate Chem.* **2009**, *20*, 95.
33. Hsiao, K.; Chapman, P.; Nilsen, S.; Eckman, C.; Harigaya, Y.; Younkin, S.; Yang, F.; Cole, G. *Science* **1996**, *274*, 99.
34. Ono, M.; Hayashi, S.; Kimura, H.; Kawashima, H.; Nakayama, M.; Saji, H. *Bioorg. Med. Chem.* **2009**, *17*, 7002.
35. Ono, M.; Watanabe, R.; Kawashima, H.; Kawai, T.; Watanabe, H.; Haratake, M.; Saji, H.; Nakayama, M. *Bioorg. Med. Chem.* **2009**, *17*, 2069.

Tissue Factor Detection for Selectively Discriminating Unstable Plaques in an Atherosclerotic Rabbit Model

Takashi Temma[1], Yuki Ogawa[1], Yuji Kuge[1,2], Seigo Ishino[1], Nozomi Takai[1], Kantaro Nishigori[1], Masashi Shiomi[3], Masahiro Ono[1], and Hideo Saji[1]

[1]Department of Patho-Functional Bioanalysis, Graduate School of Pharmaceutical Sciences, Kyoto University, Sakyo-ku, Kyoto, Japan; [2]Central Institute of Isotope Science, Hokkaido University, Kita-ku, Sapporo, Japan; and [3]Institute for Experimental Animals, Kobe University Graduate School of Medicine, Chuo-ku, Kobe, Japan

Tissue factor (TF), a transmembrane glycoprotein that acts as an essential cofactor to factor VII/VIIa, initiates the exogenous blood coagulation cascade leading to thrombin generation and subsequent thrombus formation in vivo. TF expression is closely related to plaque vulnerability, and high TF expression is shown in macrophage-rich atheromatous lesions, making TF a potential target for detecting atheromatous lesions in vivo. Thus, we prepared ^{99m}Tc-labeled anti-TF-monoclonal antibody (TF-mAb) IgG as a molecular probe and evaluated its usefulness to achieve TF-specific imaging using myocardial infarction–prone Watanabe heritable hyperlipidemic (WHHLMI) rabbits. **Methods:** Anti-TF-mAb was created using a standard hybridoma technique and was labeled by ^{99m}Tc with 6-hydrazinonicotinic acid (HYNIC) as a chelating agent to obtain ^{99m}Tc-TF-mAb. The immunoreactivity of HYNIC-TF-mAb was estimated by flow cytometry. WHHLMI and control rabbits were injected intravenously with ^{99m}Tc-TF-mAb. Twenty-four hours after the injection, the aorta was removed and radioactivity was measured. Autoradiography and histologic studies were performed using serial aorta sections. Subclass matched antibody (IgG_1) was used as a negative control. **Results:** HYNIC-TF-mAb showed 93% immunoreactivity of the anti-TF-mAb. The radioactivity accumulation in WHHLMI aortas was 6.1-fold higher than that of control rabbits. Autoradiograms showed a heterogeneous distribution of radioactivity in the intima of WHHLMI aortas. Regional radioactivity accumulation was positively correlated with TF expression density ($R = 0.64$, $P < 0.0001$). The highest radioactivity accumulation in percentage injected dose × body weight/mm^2 × 10^2 was found in atheromatous lesions (5.2 ± 1.9) followed by fibroatheromatous (2.1 ± 0.7), collagen-rich (1.8 ± 0.7), and neointimal lesions (1.8 ± 0.6). In contrast, ^{99m}Tc-IgG_1 showed low radioactivity accumulation in WHHLMI aortas that was independent of the histologic grade of lesions. **Conclusion:** The TF-detecting ability and preferential accumulation in atheromatous lesions of ^{99m}Tc-TF-mAb were demonstrated, indicating its potential for selective imaging of macrophage-rich atheromatous lesions in vivo.

Key Words: tissue factor; radioimmunodetection; thrombus; atherosclerotic plaque

J Nucl Med 2010; 51:1979–1986
DOI: 10.2967/jnumed.110.081216

Thrombus formation triggered by plaque rupture is the most important mechanism leading to the onset of acute arterial disease and ischemic sudden death. Thus, the development of a method for detecting thrombus-forming vulnerable plaques before rupture has been clinically desired to more precisely estimate risk and provide effective treatment. Although several molecular imaging probes have been investigated (*1,2*), the target molecules of such probes were not directly related to the thrombotic process.

Tissue factor (TF), a transmembrane glycoprotein that acts as an essential cofactor to factor (F) VII/VIIa, initiates the exogenous blood coagulation cascade leading to thrombin generation and subsequent thrombus formation. TF expression was identified in atherosclerotic lesions, including in endothelial cells, smooth muscle cells, monocytes, and, especially, macrophages or foam cells (*3*). In human pathologic lesions, the TF content of de novo lipid-rich plaques was higher than that of stenotic fibrous plaques (*4*), and such lipid-rich plaque tissue was 6 times more thrombogenic than fibrous plaques. In addition, our recent study also demonstrated that TF expression was closely related to plaque vulnerability, with high TF expression specifically in macrophage-rich atheromatous lesions among heterogeneous atherosclerotic lesions (*5*). Given these data, TF is a potential target for probes detecting atheromatous lesions at higher risk for rupture in vivo.

In the present study, we prepared a monoclonal antibody to TF (TF-mAb) and labeled it with ^{99m}Tc (^{99m}Tc-TF-mAb) as a molecular probe. Using an atherosclerosis model (myocardial infarction–prone Watanabe heritable hyperlipidemic [WHHLMI] rabbits) (*6*), we investigated the accumulation of ^{99m}Tc-TF-mAb in atherosclerotic lesions in comparison with histologic characteristics and evaluated the potential of ^{99m}Tc-TF-mAb as a molecular probe for detecting vulnerable atheromatous lesions.

Received Jul. 13, 2010; revision accepted Sep. 8, 2010.
For correspondence or reprints contact: Yuji Kuge, Central Institute of Isotope Science, Hokkaido University, Kita 15 Nishi 7, Kita-ku, Sapporo 060-8638, Japan.
E-mail: kuge@ric.hokudai.ac.jp

MATERIALS AND METHODS

Design and Preparation of ^{99m}Tc-TF-mAb and ^{99m}Tc-IgG$_1$

A monoclonal antibody (mouse IgG$_1$ subclass) for rabbit TF (193Ser-207Cys, extracellular domain) was established using a standard hybridoma technique. ^{99m}Tc-pertechnetate was eluted in saline solution on a daily basis from ^{99}Mo–^{99m}Tc generators (Ultra-Techne Kow; FUJIFILM RI Pharma Co., Ltd.).

Anti-TF-mAb was radiolabeled with ^{99m}Tc (^{99m}Tc-TF-mAb) after derivatization with 6-hydrazinonicotinic acid (HYNIC) (*7*), as previously reported (*8*). In brief, HYNIC-*N*-hydroxysuccinimide was reacted with TF-mAb, and the mixture was purified by size-exclusion filtration with a diafiltration membrane (Amicon Ultra 4 [molecular weight cutoff, 30,000]; Millipore Co.). An equal volume of ^{99m}Tc-(tricine)$_2$, prepared by the method of Larsen et al. (*9*), was added to the purified solution of HYNIC-TF-mAb to obtain ^{99m}Tc-TF-mAb. After purification by size-exclusion filtration with a PD-10 column, the radiochemical purity of ^{99m}Tc-TF-mAb was more than 95% by another size-exclusion filtration.

For the control study, negative control mouse IgG$_1$ (0102-01; Southern Biotechnology Associates Inc.) was used for the preparation of ^{99m}Tc-IgG$_1$. The radiochemical purity of ^{99m}Tc-IgG$_1$ was also estimated to be more than 95%.

Animals

All animal procedures were approved by the Kyoto University Animal Care Committee. Three male Japanese White rabbits (age, 3 mo) were used to obtain peritoneal macrophages. For biodistribution studies of ^{99m}Tc-TF-mAb, 5 WHHLMI rabbits (4 male, 1 female; age, 12–18 mo; mean weight ± SD, 3.4 ± 0.2 kg; supplied by the Institute for Experimental Animals, Kobe University School of Medicine, Japan) were used. Four male Japanese White rabbits (age, 3 mo; mean weight ± SD, 1.9 ± 0.2 kg) were used for the control study. For ^{99m}Tc-IgG$_1$ studies, 3 WHHLMI rabbits (1 male and 2 female; age, 11–12 mo; mean weight ± SD, 3.2 ± 0.1 kg) were used. The animals were fed standard chow and given water ad libitum.

Immunoreactivity of HYNIC-TF-mAb

Rabbit peritoneal macrophages were obtained by the method of Ishii et al. (*10*), with minor modifications. Cells were suspended at a final concentration of 2.5×10^6 cells/mL in medium A (Dulbecco's modified Eagle's medium containing 1 mM glutamine, 100 U of penicillin per milliliter, 100 mg of streptomycin per milliliter [pH 7.4], and 0.2% lactalbumin hydrolysate). Aliquots of the cell suspension were cultured in plastic petri dishes in a humidified 5% CO_2 incubator at 37°C. After 2 h, each dish was washed twice with 10 mL of medium A to remove nonadherent cells. Monolayers were cultured for 18 h at 37°C in 20 mL of medium A, and cells were washed twice with 10 mL of medium A and then used for experiments. More than 95% of the cells were viable, as determined by a trypan blue exclusion test, and almost all of the attached cells showed positive nonspecific esterase staining.

Antibodies (5 μg/mL, 100 μL; TF-mAb, HYNIC-TF-mAb, or negative control IgG$_1$) were added to the cells (10^6) and incubated for 30 min at 4°C. After cells were washed, Alexa Fluor 488 goat antimouse IgG antibody (x0931; DakoCytomation) (10 μg/mL, 100 μL) was added for 30 min at 4°C. Fluorescence levels were measured using a flow cytometer (Becton Dickinson Inc.). Data were analyzed using BD CellQuest Pro (BD Biosciences), and an immunoreactivity index was calculated as the ratio of the median fluorescence intensity for either TF-mAb or HYNIC-TF-mAb to that of negative-control IgG$_1$. Measurements were performed 3 times per rabbit using 3 Japanese White rabbits, and the ratios were expressed as mean ± SD.

Biodistribution Studies

A simple schematic of our experimental protocol is shown in Figure 1. After 12 h of fasting, rabbits were initially anesthetized with ketamine (intramuscularly, 35 mg/kg) and xylazine (intramuscularly, 5 mg/kg). Either ^{99m}Tc-TF-mAb (547–1,024 MBq,

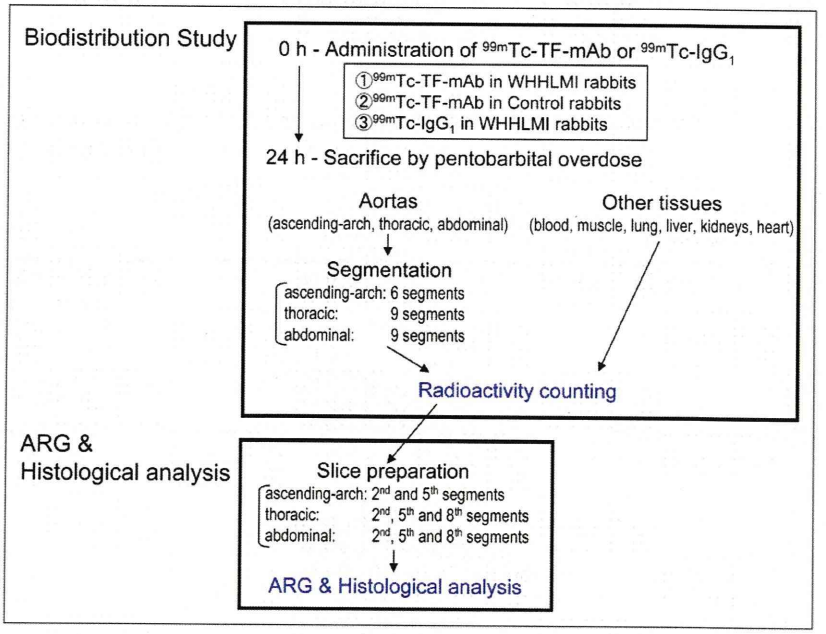

FIGURE 1. Simple schematic of this study. ARG = autoradiography.

300 μg) or ^{99m}Tc-IgG$_1$ (848–1,038 MBq, 300 μg) was injected into a marginal ear vein (5 WHHLMI rabbits and 4 control rabbits for the ^{99m}Tc-TF-mAb study, 3 WHHLMI rabbits for the ^{99m}Tc-IgG$_1$ study). Twenty-four hours after the injection, animals were sacrificed by pentobarbital overdose. The ascending-arch, thoracic, and abdominal aortas, blood, and other tissues (muscle, lung, liver, kidneys, and heart) were removed. The ascending-arch aortas were divided into 6 segments, and the thoracic and abdominal aortas were divided into 9 segments. Each segment was weighed and immediately fixed in a solution containing L-(+)-lysine hydrochloride (75 mM) and 4% paraformaldehyde in phosphate buffer (37.5 mM, pH 7.4) (*11*). The radioactivity of each sample was measured with a well-type γ-counter (1480 Wizard 3″; PerkinElmer Japan Co.). The results were expressed as the differential uptake ratio (DUR), calculated as (tissue activity/tissue weight)/(injected radiotracer activity/animal body weight), with activities given in becquerels and weights in grams. The aorta-to-blood (A/B) ratio and the aorta-to-muscle (A/M) ratio were calculated from the DUR for each tissue sample.

Autoradiography

Eight segments, the second and fifth segments of the ascending aortic arch and the second, fifth, and eighth segments from the thoracic and the abdominal aortas, from each animal were used for autoradiography studies. These segments were frozen and cut into 20-μm-thick slices with a cryomicrotome. The sections were thawed and mounted on silane-coated slides, which were then placed on a phosphor image plate (Fuji Imaging Plate BAS-MS; Fuji Photo Film) for 24 h together with a calibrated standard ($^{99m}TcO_4^-$ solution). The autoradiography images were analyzed with a computerized imaging analysis system (Bio Imaging Analyzer BAS2500 and Image Gauge Software; Fuji Photo Film). The radioactivity in each region of interest was expressed as percentage injected dose × body weight/mm^2, calculated as (radioactivity in the region of interest)/(injected radioactivity/animal body weight).

Histologic Analysis

The tissue sections used for autoradiography studies were also subjected to Azan–Mallory and hematoxylin and eosin staining. Serial sections of the slices from the autoradiography studies were subjected to immunohistochemical staining (for TF, macrophages, and smooth muscle cells) using specific antibodies and an Envision+ kit (Dako) with hematoxylin counterstaining. The antibodies used were TF-mAb (4510; American Diagnostica Inc.), rabbit macrophage–specific mAb RAM-11 (Dako), and human smooth-muscle actin–specific mAb 1A4 (Dako). Immunostaining with subclass-matched irrelevant IgG served as a negative control. Azan–Mallory and hematoxylin and eosin staining were performed by standard procedures. TF expression density was determined as a percentage of the positively stained region using a VHX digital microscope (Keyence Corp.).

Classification of Atherosclerotic Lesions

We divided atherosclerotic lesions in WHHLMI rabbits into the following 4 categories, using a classification scheme based on the recommendations of the American Heart Association (*12,13*) and Azan–Mallory and hematoxylin and eosin staining, as previously described (*14–17*): neointimal (types I–III), atheromatous (type IV), fibroatheromatous (types Va and Vb), and collagen-rich (type Vc). Supplemental Figures 1A–1P (supplemental materials are available online only at http://jnm.snmjournals.org) show representative photomicrographs of the histologic features of each atherosclerotic lesion category in WHHLMI rabbits.

Regions of interest were placed to cover each atherosclerotic lesion in the aortic section of the WHHLMI rabbit and then transferred to the corresponding autoradiography images (Supplemental Figs. 1Q–1S).

Vulnerability Index

An index of morphologic destabilization characteristics, the vulnerability index, was calculated for each lesion in the WHHLMI rabbits by the method of Shiomi et al. (*18*). The vulnerability index was defined as the ratio of the lipid component area (macrophages and extracellular lipid deposits) to the fibromuscular component area (smooth muscle cells and collagen fibers). Collagen fibers and extracellular lipid deposits (extracellular vacuoles and lacunae) were determined with Azan–Mallory stain-

TABLE 1
Accumulation Levels of ^{99m}Tc-TF-mAb and ^{99m}Tc-IgG$_1$ in Aortic Segments of Control and WHHLMI Rabbits at 24 Hours After Injection

Segments	^{99m}Tc-TF-mAb		^{99m}Tc-IgG$_1$, WHHLMI
	Control	WHHLMI	
Ascending arch	0.60 ± 0.05	3.08 ± 0.57*†	2.05 ± 0.42*
Thoracic	0.51 ± 0.11	3.07 ± 1.44*‡	1.60 ± 0.44*
Abdominal	0.35 ± 0.06	2.49 ± 0.64*‡	0.76 ± 0.16*
Total	0.47 ± 0.04	2.86 ± 0.85*‡	1.40 ± 0.24*
Blood	4.0 ± 0.6	7.5 ± 0.0*	7.1 ± 0.7§
Femoral muscle	0.6 ± 0.5	0.3 ± 0.2	0.4 ± 0.1
Aorta-to-blood ratio	0.12 ± 0.02	0.38 ± 0.09*‡	0.20 ± 0.02*
Aorta-to-muscle ratio	1.0 ± 0.6	19.3 ± 19.1*‡	4.0 ± 0.4*

*$P < 0.0001$ vs. control rabbits in ^{99m}Tc-TF-mAb study.
†$P < 0.001$ vs. WHHLMI rabbits in ^{99m}Tc-IgG$_1$ study.
‡$P < 0.0001$ vs. WHHLMI rabbits in ^{99m}Tc-IgG$_1$ study.
§$P < 0.001$, vs. control rabbits in ^{99m}Tc-TF-mAb study.
Data are represented as mean ± SD of DUR.

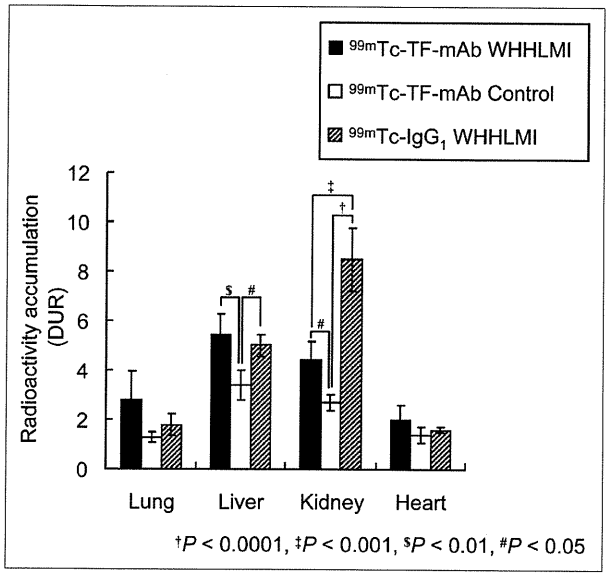

FIGURE 2. Radioactivity distribution in lung, liver, kidneys, and heart. Data are mean ± SD. †$P < 0.0001$. ‡$P < 0.001$. $$P < 0.01$. #$P < 0.05$.

ing. Macrophages and smooth muscle cells were determined with immunohistochemical staining (*17*).

Statistical Analysis

Data are presented as mean ± SD. Statistical analysis was performed with the Mann–Whitney *U* test to compare aortic segments of WHHLMI and control rabbits (Table 1). Radioactivity that accumulated in nontargeted organs among antibodies and animals was compared using 1-way ANOVA, with post hoc analysis by the Holm test (Fig. 2). Correlation coefficients were assessed by Spearman rank correlation coefficients (Fig. 3). Lesion types were compared using the Kruskal–Wallis test, with post hoc analysis by the Scheffé test (Fig. 4). A 2-tailed value of *P* less than 0.05 was considered statistically significant.

RESULTS

Immunoreactivity of HYNIC-TF-mAb

Using fluorescent-activated cell sorter analysis of rabbit peritoneal macrophages, we could clearly distinguish the signals of TF-mAb and HYNIC-TF-mAb from that of the negative control IgG_1. The median fluorescence intensity ratios of TF-mAb and HYNIC-TF-mAb to control IgG_1 were 2.90 ± 0.06 and 2.69 ± 0.11, respectively, and the difference between the labeled and unlabeled TF antibodies was not statistically significant.

Biodistribution Studies

Accumulation levels of ^{99m}Tc-TF-mAb and ^{99m}Tc-IgG_1 in the aortic segments of WHHLMI and control rabbits are summarized in Table 1. The accumulation level of ^{99m}Tc-TF-mAb in each aortic segment of WHHLMI rabbits (ascending arch, 3.08 ± 0.57 DUR; thoracic, 3.07 ± 1.44 DUR; and abdominal, 2.49 ± 0.64 DUR) was 5.1- to 7.1-fold higher than that of control rabbits (ascending arch, 0.60 ± 0.05 DUR; thoracic, 0.51 ± 0.11 DUR; and abdominal, 0.35 ± 0.06 DUR), and the differences were significant in each case. Blood-pool radioactivity levels of ^{99m}Tc-TF-mAb at 24 h were 7.5 ± 0.0 and 4.0 ± 0.6 DUR in WHHLMI and control rabbits, respectively. A/B and A/M ratios were significantly higher in WHHLMI rabbits than in control rabbits (A/B, 0.38 ± 0.09 in WHHLMI and 0.12 ± 0.02 in control rabbits; A/M, 19.3 ± 19.1 in WHHLMI and 1.0 ± 0.6 in control rabbits). In addition, the level of ^{99m}Tc-TF-mAb accumulation in WHHLMI rabbit aortas was 1.5- to 3.3-fold higher than the level of ^{99m}Tc-IgG_1 accumulation, and the differences were significant.

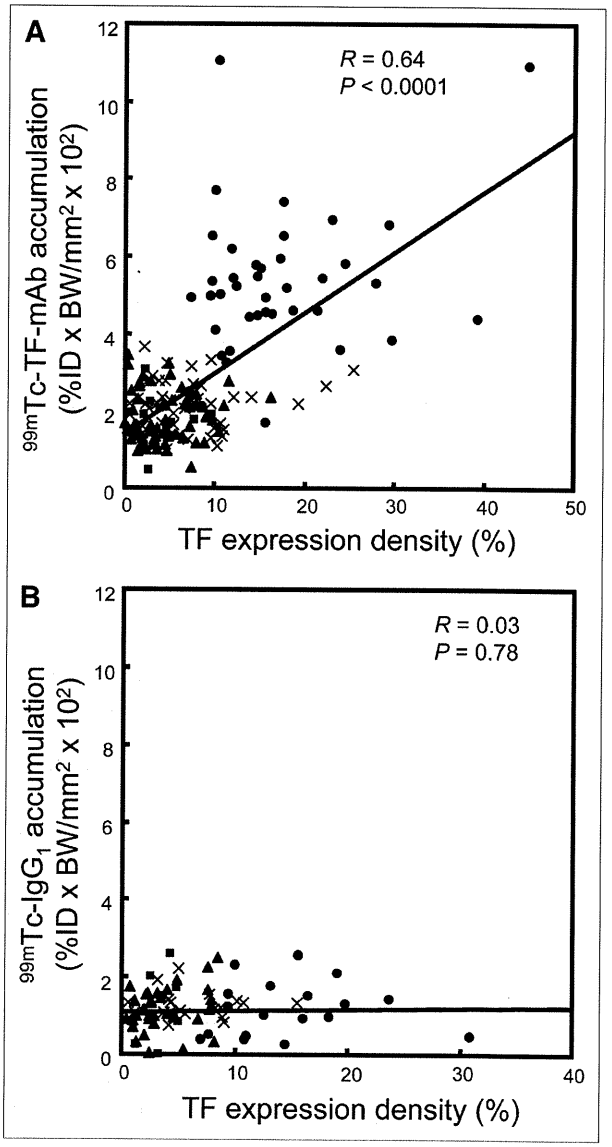

FIGURE 3. Regression analyses of TF expression density with ^{99m}Tc-TF-mAb (A) and ^{99m}Tc-IgG_1 (B) accumulation. ■ = neointimal lesion; ● = atheromatous lesion; × = fibroatheromatous lesion; ▲ = collagen-rich lesion.

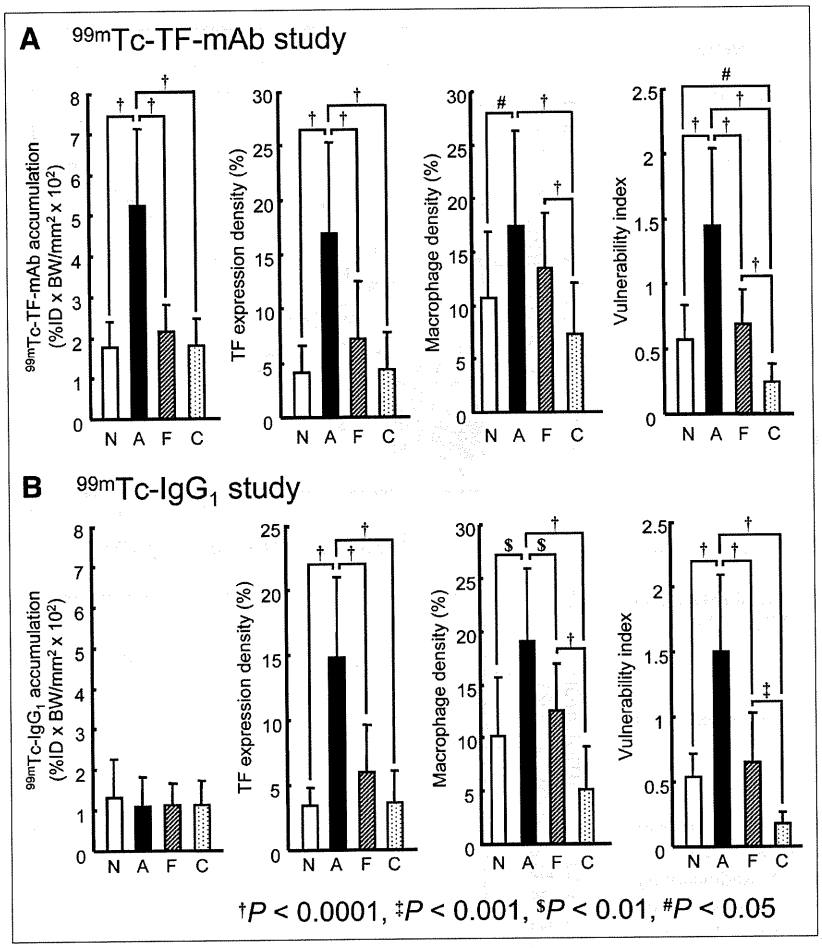

FIGURE 4. Distribution profiles of radioactivity accumulation, TF expression, macrophage density, and vulnerability index in atherosclerotic lesions in ^{99m}Tc-TF-mAb (A) and ^{99m}Tc-IgG$_1$ (B) study. A = atheromatous lesions; C = collagen-rich lesions; F = fibroatheromatous lesions; N = neointimal lesions. Data are represented as mean ± SD.

Relatively high radioactivity accumulations were found in the liver and kidneys of all 3 groups (Fig. 2). We observed that the ^{99m}Tc-TF-mAb cleared rather more slowly from the bodies of WHHLMI rabbits than from control rabbits.

Regional Distribution of ^{99m}Tc-TF-mAb, in Comparison with TF Expression

In the autoradiography study, heterogeneous ^{99m}Tc-TF-mAb accumulation was observed in the intima of WHHLMI rabbit aortas (Fig. 5B), whereas no marked accumulation was found in the aortas of control rabbits (Fig. 5A). Variable TF expression was detected in the intimal regions of the WHHLMI rabbit aorta (Figs. 5D, 5F, and 5G). Higher accumulation levels of ^{99m}Tc-TF-mAb were found in regions with high TF expression, whereas lower accumulation was observed in regions with low TF expression (Fig. 5, compare 5B with 5F and 5G). Consequently, regional ^{99m}Tc-TF-mAb accumulation levels in the aorta section were positively correlated with TF expression density in WHHLMI rabbits ($R = 0.64$, $P < 0.0001$) (Fig. 3A). No obvious TF expression was observed in the aorta of control rabbits (Figs. 5C, 5E, and 3B).

Relationship Between ^{99m}Tc-TF-mAb Accumulation and Histologic Characteristics

The plaques were categorized according to histopathologic classification criteria as follows: neointimal ($n = 12$ for ^{99m}Tc-TF-mAb study and $n = 7$ for ^{99m}Tc-IgG$_1$ study), atheromatous ($n = 40$ for ^{99m}Tc-TF-mAb study and $n = 20$ for ^{99m}Tc-IgG$_1$ study), fibroatheromatous ($n = 43$ for ^{99m}Tc-TF-mAb study and $n = 21$ for ^{99m}Tc-IgG$_1$ study), and collagen-rich ($n = 62$ for ^{99m}Tc-TF-mAb study and $n = 36$ for ^{99m}Tc-IgG$_1$ study). No lesions showed hemorrhage, plaque rupture, or thrombi (type VI). The level of ^{99m}Tc-TF-mAb accumulation was dependent on the histologic grade of the lesions (Fig. 4A) and was prominently and significantly the highest ($P < 0.0001$) in atheromatous lesions (type IV), compared with other lesions. The accumulation level of ^{99m}Tc-TF-mAb was 3.0-, 2.4-, and 2.9-fold higher in atheromatous lesions than in neointimal, fibroatheromatous, and collagen-rich lesions, respectively. The vulnerability index was also the highest in atheromatous lesions, followed in decreasing order by fibroatheromatous, neointimal, and collagen-rich lesions. Consequently, the highest level of ^{99m}Tc-TF-mAb accumulation and the highest vulnerability

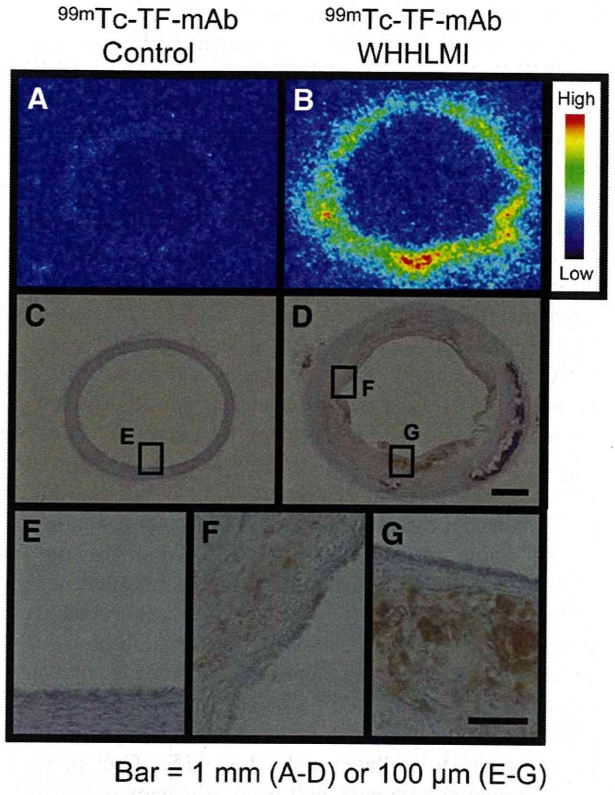

FIGURE 5. Regional distribution of ^{99m}Tc-TF-mAb and TF expression in aortic sections. Autoradiogram (A and B) and TF immunohistochemical staining (C–G) of control (C and E) and WHHLMI rabbits (D, F, and G). (E–G) High-magnification images of TF immunohistochemical staining in regions depicted in C and D. Identical color window was applied to both autoradiographic images (A and B). Bar = 1 mm (A–D) and 100 μm (E–G).

index were both observed in atheromatous lesions. In contrast, ^{99m}Tc-IgG$_1$ accumulation in lesions was low and did not correlate with the histologic grade of lesions, with no significant differences among the lesion types (Fig. 4B).

DISCUSSION

In the present study, we designed a new imaging agent, ^{99m}Tc-TF-mAb, for the purpose of discriminating atherosclerotic lesions at higher risk for rupture (thrombogenic atheromatous lesions) from more stable lesions and evaluated the potential of ^{99m}Tc-TF-mAb using an atherosclerotic rabbit model. Our major findings are that a positive correlation was demonstrated between regional ^{99m}Tc-TF-mAb accumulation and TF expression density in atherosclerotic lesions of WHHLMI rabbits but not with ^{99m}Tc-IgG$_1$ and that significantly higher ^{99m}Tc-TF-mAb accumulation was found in grade IV, more vulnerable atheromatous lesions, than in neointimal lesions or other more stable lesions. Thus, we demonstrate the potential of ^{99m}Tc-TF-mAb for molecular imaging of TF expression and selectively detecting atheromatous plaques at higher risk for rupture.

Immunoreactivity and Specificity of ^{99m}Tc-TF-mAb

Immunoreactivity, specificity, and detectable but functionally silent labeling are indispensable prerequisites of in vivo molecular imaging probes using immunodetection. In this study, flow cytometric analyses indicated that modification of TF-mAb with HYNIC did not significantly affect the immunoreactivity of the original TF-mAb. In addition, autoradiography and immunohistochemical studies showed that ^{99m}Tc-TF-mAb accumulation in atherosclerotic lesions correlated well with TF expression density, which was higher in atheromatous lesions, as expected (Figs. 3A and 4A). Further, contrary to the results with ^{99m}Tc-TF-mAb (Fig. 4A), the results with ^{99m}Tc-IgG$_1$ (Fig. 4B) showed that accumulation of ^{99m}Tc-labeled nonspecific IgG in atheromatous lesions was not significantly different from that in other types of lesions (i.e., neointimal, fibroatheromatous, and collagen-rich lesions). These findings strongly suggest the potential of ^{99m}Tc-TF-mAb to specifically recognize TF in vivo.

TF as a Target Molecule for Plaque Imaging

TF, selected as a target molecule for molecular imaging in this study, initiates the exogenous blood coagulation cascade leading to thrombus formation in vivo and represents a good marker for late-stage vulnerable lesions. TF in atherosclerotic lesions was identified in several cell types, such as endothelial cells, smooth muscle cells, monocytes, macrophages, and foam cells (*3*), similar to lectinlike oxidized low-density lipoprotein receptor 1 (LOX-1). TF expression is reported to be increased in the later stages of atheromatous progression and thus was selectively detected in atheromatous lesions in this report (Fig. 4). These findings are comparable to those of our previous immunohistochemical study (*5*) and another human study (*4*). On these bases, TF should be a potential target for detecting atheromatous plaques at higher risk for rupture in vivo. To our knowledge, this is the first report of the development of an in vivo TF imaging probe.

On the other hand, a series of imaging agents has targeted fibrin and factor XIII in thrombi using antibodies or peptides (*1*), with at least partial success. In the blood-coagulation cascade, TF initiates the system, and factor XIII covalently cross-links fibrin polymers and renders the thrombus more resistant to lysis. Therefore, ^{99m}Tc-TF-mAb will be useful for the early detection of the cascade, and fibrin and factor XIII imaging probes can detect later stages and thrombi themselves. In this study, ^{99m}Tc-TF-mAb corresponded with TF expression and showed preferential accumulation in atheromatous lesions and in lesions with increased vulnerability. Although further studies are required to investigate which target molecules in the cascade are most appropriate to estimate how unstable or vulnerable a plaque is in vivo, TF is a potential target. Furthermore, because great efforts have been made in the development of anticoagulation and antiplatelet pharmaceuticals for the treatment of atherosclerosis and

hyperlipidemia, effective imaging probes to target blood-coagulation cascades are also required for efficient drug development.

Limitations of ^{99m}Tc-TF-mAb

One drawback of ^{99m}Tc-TF-mAb is its relatively slow clearance from the blood, which is an intrinsic problem of molecular probes using antibodies. Recent advances in antibody engineering, however, should provide a promising solution for this issue. Radioprobes derived from low-molecular-weight polypeptides or compounds, small recombinant antibody fragments (Fab, scFv), engineered variants (diabodies, triabodies, minibodies, and single-domain antibodies), or pretargeting antibody methods show rapid clearance of radioactivity from the circulation (*19–21*). Image-subtraction techniques (*22–24*) or kinetic model analysis (*25,26*) may also help solve this issue. Accordingly, ^{99m}Tc-TF-mAb or its derivatives have great potential as in vivo molecular imaging probes and deserve further investigation.

A higher renal accumulation of ^{99m}Tc-IgG$_1$ than of ^{99m}Tc-TF-mAb was observed in WHHLMI rabbits. Although an exact mechanistic explanation for this significant difference is not clear, several other investigators have also reported a relatively high renal accumulation after the injection of radiolabeled mAbs (*27–29*). Because we evaluated the biodistribution 24 h after the injection (relatively late phase), renal accumulation may be ascribed to metabolic or degradation products of ^{99m}Tc-labeled antibodies (*30*). Thus, further ex vivo metabolite analysis studies could help to clarify the mechanism. In addition, it is known that the excretion system of WHHLMI rabbits is compromised (*31*), which could alter the renal accumulation of tracers. On the other hand, although a certain degree of TF expression was observed in glomeruli (*32*), this could not be a reason for the higher renal accumulation of ^{99m}Tc-IgG$_1$.

Recently, the focus of anticoagulant research has turned to inhibition of the TF-FVIIa complex, and many pharmaceutical industry research programs have attempted to discover TF-FVIIa complex inhibitors (*33*). Studies in monkeys have indicated that inhibition of the TF-FVIIa complex, compared with other anticoagulants that inhibit thrombin or FXa, results in an improved profile . It is well known that the pathways for blood coagulation are interdependent, and the initiation, amplification, and propagation stages are closely regulated by positive and negative feedback loops. Thus, repeated doses of anticoagulants might increase the expression of ineffective (silent) TF complex in plaques because of such feedback processes independent of the antiatherosclerotic effect, although a lowering of net TF expression would be expected. The TF antibody we established in this study recognizes 193Ser-207Cys in the extracellular domain, which is distant from the protein sites related to complex formation with FVIIa. Therefore, the ^{99m}Tc-TF-mAb we developed can estimate the net TF expression in plaques, providing a useful tool to investigate the effect of such anticoagulants in vivo.

Comparison with Other Imaging Probes

In the search for suitable molecular probes to assess atherosclerotic lesion characteristics, many targets, including macrophage activity, angiogenesis, apoptosis, and cell tracking (monocyte, stem cell, lymphocyte), have been assessed (*1,2,34–36*). However, the usefulness of these probes is still under preliminary investigation, except for ^{18}F-FDG, a marker of inflammation, and ^{99m}Tc-annexin A5, a marker of ongoing apoptotic cell death, which are currently in clinical studies. In previous studies, we evaluated macrophage imaging using ^{18}F-FDG (*11*) and also ^{99m}Tc-LOX-1-mAb (*17*), which targets a scavenger receptor highly expressed on macrophages and foam cells and showed the usefulness for detection of atherosclerotic lesions. However, ^{18}F-FDG accumulated in relatively stable lesions because of the presence of macrophages in such lesions, as also seen in this report (Fig. 4). We also previously showed a certain degree of LOX-1 expression in relatively stable lesions with ^{99m}Tc-LOX-1-mAb. As for ^{99m}Tc-annexin A5, the accumulation ratios of atheromatous lesions to other lesions of ^{99m}Tc-TF-mAb (atheromatous to neointimal, 3.0; atheromatous to fibroatheromatous, 2.4; and atheromatous to collagen-rich, 2.9) were markedly higher than those of ^{99m}Tc-annexin A5 (atheromatous to neointimal,1.3; atheromatous to fibroatheromatous, 1.3; atheromatous to collagen-rich, 1.8) (*15*). Our previous study in apolipoprotein E–null mice also showed relatively high ^{18}F-FDG accumulation levels in early lesions, resulting in lower accumulation ratios for advanced to early lesions in comparison with ^{99m}Tc-annexin A5 (*37*). Thus, the desirable features of ^{99m}Tc-TF-mAb further confirm its potential as a molecular probe for detecting atheromatous lesions at higher risk for rupture.

CONCLUSION

In this study, we succeeded in determining TF expression using ^{99m}Tc-TF-mAb in WHHLMI rabbits. Consequently, we demonstrated prominently higher accumulation of ^{99m}Tc-TF-mAb in grade IV atheroma. These findings strongly indicate that molecular imaging of TF should provide clinically useful information on the thrombogenicity of atherosclerotic plaques.

ACKNOWLEDGMENTS

This work was partly supported by a grant-in-aid for general scientific research from the Ministry of Education, Culture, Sports, Science and Technology of Japan and from the Japan Society for the Promotion of Science and by a research grant from the Association for Nuclear Technology in Medicine and Takeda Science Foundation.

REFERENCES

1. Shaw SY. Molecular imaging in cardiovascular disease: targets and opportunities. *Nat Rev Cardiol.* 2009;6:569–579.
2. Saraste A, Nekolla SG, Schwaiger M. Cardiovascular molecular imaging: an overview. *Cardiovasc Res.* 2009;83:643–652.

3. Moons AH, Levi M, Peters RJ. Tissue factor and coronary artery disease. *Cardiovasc Res.* 2002;53:313–325.
4. Jeanpierre E, Le Tourneau T, Six I, et al. Dietary lipid lowering modifies plaque phenotype in rabbit atheroma after angioplasty: a potential role of tissue factor. *Circulation.* 2003;108:1740–1745.
5. Kuge Y, Kume N, Ishino S, et al. Prominent lectin-like oxidized low density lipoprotein (LDL) receptor-1 (LOX-1) expression in atherosclerotic lesions is associated with tissue factor expression and apoptosis in hypercholesterolemic rabbits. *Biol Pharm Bull.* 2008;31:1475–1482.
6. Shiomi M, Ito T, Yamada S, Kawashima S, Fan J. Development of an animal model for spontaneous myocardial infarction (WHHLMI rabbit). *Arterioscler Thromb Vasc Biol.* 2003;23:1239–1244.
7. Abrams MJ, Juweid M, tenKate CI, et al. Technetium-99m-human polyclonal IgG radiolabeled via the hydrazino nicotinamide derivative for imaging focal sites of infection in rats. *J Nucl Med.* 1990;31:2022–2028.
8. Ono M, Arano Y, Mukai T, et al. Plasma protein binding of ^{99m}Tc-labeled hydrazino nicotinamide derivatized polypeptides and peptides. *Nucl Med Biol.* 2001;28:155–164.
9. Larsen SK, Solomon HF, Caldwell G, Abrams MJ. [^{99m}Tc]tricine: a useful precursor complex for the radiolabeling of hydrazinonicotinate protein conjugates. *Bioconjug Chem.* 1995;6:635–638.
10. Ishii K, Kita T, Kume N, Nagano Y, Kawai C. Uptake of acetylated LDL by peritoneal macrophages obtained from normal and Watanabe heritable hyperlipidemic rabbits, an animal model for familial hypercholesterolemia. *Biochim Biophys Acta.* 1988;962:387–389.
11. Ogawa M, Ishino S, Mukai T, et al. ^{18}F-FDG accumulation in atherosclerotic plaques: immunohistochemical and PET imaging study. *J Nucl Med.* 2004;45:1245–1250.
12. Stary HC, Chandler AB, Glagov S, et al. A definition of initial, fatty streak, and intermediate lesions of atherosclerosis: a report from the Committee on Vascular Lesions of the Council on Arteriosclerosis, American Heart Association. *Circulation.* 1994;89:2462–2478.
13. Stary HC, Chandler AB, Dinsmore RE, et al. A definition of advanced types of atherosclerotic lesions and a histological classification of atherosclerosis: a report from the Committee on Vascular Lesions of the Council on Arteriosclerosis, American Heart Association. *Circulation.* 1995;92:1355–1374.
14. Kobayashi S, Inoue N, Ohashi Y, et al. Interaction of oxidative stress and inflammatory response in coronary plaque instability: important role of C-reactive protein. *Arterioscler Thromb Vasc Biol.* 2003;23:1398–1404.
15. Ishino S, Kuge Y, Takai N, et al. ^{99m}Tc-Annexin A5 for noninvasive characterization of atherosclerotic lesions: imaging and histological studies in myocardial infarction-prone Watanabe heritable hyperlipidemic rabbits. *Eur J Nucl Med Mol Imaging.* 2007;34:889–899.
16. Shiomi M, Ito T, Hirouchi Y, Enomoto M. Stability of atheromatous plaque affected by lesional composition: study of WHHL rabbits treated with statins. *Ann N Y Acad Sci.* 2001;947:419–423.
17. Ishino S, Mukai T, Kuge Y, et al. Targeting of lectinlike oxidized low-density lipoprotein receptor 1 (LOX-1) with ^{99m}Tc-labeled anti-LOX-1 antibody: potential agent for imaging of vulnerable plaque. *J Nucl Med.* 2008;49:1677–1685.
18. Shiomi M, Ito T, Hirouchi Y, Enomoto M. Fibromuscular cap composition is important for the stability of established atherosclerotic plaques in mature WHHL rabbits treated with statins. *Atherosclerosis.* 2001;157:75–84.
19. Huhalov A, Chester KA. Engineered single chain antibody fragments for radioimmunotherapy. *Q J Nucl Med Mol Imaging.* 2004;48:279–288.
20. Sharkey RM, Karacay H, Cardillo TM, et al. Improving the delivery of radionuclides for imaging and therapy of cancer using pretargeting methods. *Clin Cancer Res.* 2005;11:7109s–7121s.
21. Sano K, Temma T, Kuge Y, et al. Radioimmunodetection of membrane type-1 matrix metalloproteinase relevant to tumor malignancy with a pre-targeting method. *Biol Pharm Bull.* 2010;33:1589–1595.
22. Temma T, Iida H, Hayashi T, et al. Quantification of regional myocardial oxygen metabolism in normal pigs using positron emission tomography with injectable ^{15}O-O_2. *Eur J Nucl Med Mol Imaging.* 2010:37:377–385.
23. Yamamoto Y, de Silva R, Rhodes CG, et al. Noninvasive quantification of regional myocardial metabolic rate of oxygen by $^{15}O_2$ inhalation and positron emission tomography: experimental validation. *Circulation.* 1996;94:808–816.
24. Iida H, Rhodes CG, Araujo LI, et al. Noninvasive quantification of regional myocardial metabolic rate for oxygen by use of $^{15}O_2$ inhalation and positron emission tomography: theory, error analysis, and application in humans. *Circulation.* 1996;94:792–807.
25. Watabe H, Ikoma Y, Kimura Y, Naganawa M, Shidahara M. PET kinetic analysis: compartmental model. *Ann Nucl Med.* 2006;20:583–588.
26. Ikoma Y, Watabe H, Shidahara M, Naganawa M, Kimura Y. PET kinetic analysis: error consideration of quantitative analysis in dynamic studies. *Ann Nucl Med.* 2008;22:1–11.
27. Rogers BE, Anderson CJ, Connett JM, et al. Comparison of four bifunctional chelates for radiolabeling monoclonal antibodies with copper radioisotopes: biodistribution and metabolism. *Bioconjug Chem.* 1996;7:511–522.
28. Sugimoto K, Nishimoto N, Kishimoto T, Yoshizaki K, Nishimura T. Imaging of lesions in a murine rheumatoid arthritis model with a humanized anti-interleukin-6 receptor antibody. *Ann Nucl Med.* 2005;19:261–266.
29. D'Alessandria C, Malviya G, Viscido A, et al. Use of a ^{99m}Tc labeled anti-TNFα monoclonal antibody in Crohn's disease: in vitro and in vivo studies. *Q J Nucl Med Mol Imaging.* 2007;51:334–342.
30. Akizawa H, Arano Y. Altering pharmacokinetics of radiolabeled antibodies by the interposition of metabolizable linkages: metabolizable linkers and pharmacokinetics of monoclonal antibodies. *Q J Nucl Med.* 2002;46:206–223.
31. Campean V, Neureiter D, Varga I, et al. Atherosclerosis and vascular calcification in chronic renal failure. *Kidney Blood Press Res.* 2005;28:280–289.
32. Drake TA, Morrissey JH, Edgington TS. Selective cellular expression of tissue factor in human tissues: implications for disorders of hemostasis and thrombosis. *Am J Pathol.* 1989;134:1087–1097.
33. Prezelj A, Anderluh PS, Peternel L, Urleb U. Recent advances in serine protease inhibitors as anticoagulant agents. *Curr Pharm Des.* 2007;13:287–312.
34. Davies JR, Rudd JH, Weissberg PL, Narula J. Radionuclide imaging for the detection of inflammation in vulnerable plaques. *J Am Coll Cardiol.* 2006;47(8, suppl):C57–C68.
35. Jaffer FA, Libby P, Weissleder R. Molecular and cellular imaging of atherosclerosis: emerging applications. *J Am Coll Cardiol.* 2006;47:1328–1338.
36. Rudd JH, Hyafil F, Fayad ZA. Inflammation imaging in atherosclerosis. *Arterioscler Thromb Vasc Biol.* 2009;29:1009–1016.
37. Zhao Y, Kuge Y, Zhao S, et al. Comparison of ^{99m}Tc-annexin A5 with ^{18}F-FDG for the detection of atherosclerosis in ApoE−/− mice. *Eur J Nucl Med Mol Imaging.* 2007;34:1747–1755.

Erratum

In the article "^{18}F-FDG PET After 2 Cycles of ABVD Predicts Event-Free Survival in Early and Advanced Hodgkin Lymphoma," by Cerci et al. (*J Nucl Med.* 2010;51:1337–1343), Figure 4 contained a mistake. The graph of event-free survival in patients with a low International Prognostic Score should indicate that 10 of 18 patients (not 3 of 30) were PET2-positive. The authors regret the error.

Radioimmunodetection of Membrane Type-1 Matrix Metalloproteinase Relevant to Tumor Malignancy with a Pre-targeting Method

Kohei SANO,[a] Takashi TEMMA,[a] Yuji KUGE,*[,a,b,c] Takashi KUDO,[a] Junko KAMIHASHI,[a] Songji ZHAO,[b] and Hideo SAJI[a]

[a] *Department of Patho-Functional Bioanalysis, Graduate School of Pharmaceutical Sciences, Kyoto University; 46–29 Yoshida Shimoadachi-cho, Sakyo-ku, Kyoto 606–8501, Japan:* [b] *Department of Tracer Kinetics & Bioanalysis, Graduate School of Medicine, Hokkaido University; and* [c] *Central Institute of Isotope Science, Hokkaido University; Kita 15 Nishi 7, Kita-ku, Sapporo 060–8638, Japan.* Received April 5, 2010; accepted June 28, 2010; published online June 30, 2010

Since membrane type-1 matrix metalloproteinase (MT1-MMP) is exclusively expressed in tumors and is closely associated with metastasis and invasion, MT1-MMP is a potential target of radiotracers for the evaluation of tumor malignancy. In this study, we planned to visualize MT1-MMP *in vivo* by a two-step pre-targeting strategy using a streptavidin (SAv)-biotin system combined with anti-MT1-MMP monoclonal immunoglobulin (IgG) (anti-MT1-MMP monoclonal antibody (mAb)). Streptavidinylated anti-MT1-MMP mAb was synthesized by reacting biotinylated anti-MT1-MMP mAb with SAv. In the pre-targeting study, FM3A mouse breast carcinoma-implanted mice were injected with anti-MT1-MMP mAb-SAv, followed 72 h later with radioiodinated biotin, (3-[$^{123/125}$I]iodobenzoyl)norbiotinamide ($^{123/125}$I-IBB). Biodistribution and imaging (single photon emission computed tomography (SPECT)/CT) data were collected at several time points in the 24 h period following introduction of the tracer. The comparison groups were injected with ^{125}I-IBB alone or with ^{125}I-IBB pre-targeted with negative control IgG-SAv. In the pre-targeting study for MT1-MMP, within 1 h of tracer injection, rapid tumor uptake and abrupt clearance from the blood of radioactivity (2.22, 0.87% injected dose/g at 1 h) were observed. The tumor to blood (T/B) radioactivity ratios were significantly higher than those from mice dosed with the pre-targeting negative control ($p<0.0001$). ^{125}I-IBB alone did not accumulate in tumors. SPECT/CT image analysis of FM3A bearing mice showed high-contrast tumor images after 3 h with minimal blood-pool activity. The present study that uses a pre-targeting method showed high T/B radioactivity ratios and clear tumor images of MT1-MMP. This imaging method may be useful for the clinical diagnosis of malignant tumors.

Key words membrane type-1 matrix metalloproteinase; pre-targeting; non-invasive imaging; streptavidin; biotin; malignant tumor

Tumor malignancy is closely associated with the poor prognosis in cancer patients. Thus, accurate and sensitive diagnosis for detecting the tumor malignancy is required to provide the optimal therapeutic regimen to the patients. Nuclear medical techniques such as single photon emission computed tomography (SPECT) and positron emission tomography (PET) are non-invasive and have the potential to provide sensitive diagnoses by detecting gamma rays emitted from a radiolabeled probe injected into the body. Thus, a radiolabeled probe targeted to a biological molecule relevant to tumor malignancy can be a useful tool for detecting the malignant tumors.

Matrix metalloproteinases (MMPs), classified as secreted MMPs and membrane-associated MMPs (membrane type MMPs, MT-MMPs) based on their structures,[1)] play important roles in tumor growth, invasion, and metastasis by degrading most of the components in the extracellular matrix.[2)] Membrane type-1 MMP (MT1-MMP) in particular is considered to be closely associated with tumor malignancy. Indeed, recent studies have shown that MT1-MMP activates MMP-2, an effector protease that operates downstream of MT1-MMP.[1,3—6)] In addition, expression of MT1-MMP is localized to tumor tissues[1)] and increases in the early stages of tumorigenesis.[7)] Thus, MT1-MMP is a potential target for imaging malignant tumors at an early phase in their development.

Recently, we proposed ^{99m}Tc-labeled anti-MT1-MMP monoclonal immunoglobulin (IgG) (^{99m}Tc-anti-MT1-MMP monoclonal antibody (mAb)) as a novel MT1-MMP probe and demonstrated its effectiveness for evaluating the malignancy of breast tumors in rodent models.[8)] However, the blood clearance of ^{99m}Tc-anti-MT1-MMP mAb was not fast enough to obtain a high tumor to blood (T/B) ratio, an indicator of availability of radiotracer for *in vivo* imaging, during the first hours following administration. The T/B ratio remained low at 48 h post-injection, which prevents the achievement of MT1-MMP imaging *in vivo*. For future clinical applications, this probe should be modified to improve the MT1-MMP imaging sensitivity and to provide earlier post-injection imaging.

For this purpose, we planed to use a pre-targeting method combined with the anti-MT1-MMP mAb. The pre-targeting method, extensively studied in the field of radioimmunotherapy, can provide selective accumulation of radioactivity to the targeted organ and a high signal-to-noise (S/N) ratio during the first hours following administration.[9,10)] Recently, publications have reported that the pre-targeting method, utilizing an interaction between bispecific antibodies and haptens, is applicable to *in vivo* molecular imaging.[11,12)] Here, we exploited a streptavidin–biotin system possessing high affinity ($K_d=10^{-15}$ M)[13)] for *in vivo* binding of pre- and post-administered compounds and applied this pre-targeting method to MT1-MMP imaging.

This study sought to determine the effectiveness of a pre-targeting protocol (streptavidinylated anti-MT1-MMP mAb and radiolabeled biotin) for MT1-MMP imaging shortly after administration of a radiolabeled probe, through biodistribution studies and *in vivo* SPECT imaging. Among tumor types, breast cancer remains a predominant cause of death in women despite advances in treatment, especially in cases where distant metastases occur.[14)] This motivated us to select

* To whom correspondence should be addressed. e-mail: kuge@ric.hokudai.ac.jp